(12) INTERNATIONAL APPLICATION PUBLISHED UNDER THE PATENT COOPERATION TREATY (PCT)

(19) World Intellectual Property Organization
International Bureau

(43) International Publication Date
28 May 2015 (28.05.2015)

WIPO | PCT

(10) International Publication Number
WO 2015/077355 A1

(51) International Patent Classification:
*G02B 21/00* (2006.01)

(21) International Application Number:
PCT/US2014/066437

(22) International Filing Date:
19 November 2014 (19.11.2014)

(25) Filing Language: English

(26) Publication Language: English

(30) Priority Data:
61/906,238 19 November 2013 (19.11.2013) US

(71) Applicant: **WASHINGTON UNIVERSITY** [US/US]; One Brookings Drive, St. Louis, Missouri 63130 (US).

(72) Inventors: **WANG, Lihong;** Washington University, One Brookings Drive, St. Louis, Missouri 63130 (US). **WANG, Lidai;** Washington Unviersity, One Brookings Drive, St. Louis, Missouri 63130 (US). **ZHANG, Chi;** Washington University, One Brookings Drive, St. Louis, Missouri 63130 (US). **LAI, Puxiang;** Washington University, One Brookings Drive, St. Louis, Missouri 63130 (US). **TAY, Jian Wei;** Washington University, One Brookings Drive, St. Louis, Missouri 63130 (US).

(74) Agents: **BRENNAN, Patrick, E.** et al; ARMSTRONG TEASDALE LLP, 7700 Forsyth Blvd., Suite 1800, St. Louis, Missouri 63105 (US).

(81) Designated States *(unless otherwise indicated, for every kind of national protection available):* AE, AG, AL, AM, AO, AT, AU, AZ, BA, BB, BG, BH, BN, BR, BW, BY, BZ, CA, CH, CL, CN, CO, CR, CU, CZ, DE, DK, DM, DO, DZ, EC, EE, EG, ES, FI, GB, GD, GE, GH, GM, GT, HN, HR, HU, ID, IL, IN, IR, IS, JP, KE, KG, KN, KP, KR, KZ, LA, LC, LK, LR, LS, LU, LY, MA, MD, ME, MG, MK, MN, MW, MX, MY, MZ, NA, NG, NI, NO, NZ, OM, PA, PE, PG, PH, PL, PT, QA, RO, RS, RU, RW, SA, SC, SD, SE, SG, SK, SL, SM, ST, SV, SY, TH, TJ, TM, TN, TR, TT, TZ, UA, UG, US, UZ, VC, VN, ZA, ZM, ZW.

(84) Designated States *(unless otherwise indicated, for every kind of regional protection available):* ARIPO (BW, GH, GM, KE, LR, LS, MW, MZ, NA, RW, SD, SL, ST, SZ, TZ, UG, ZM, ZW), Eurasian (AM, AZ, BY, KG, KZ, RU, TJ, TM), European (AL, AT, BE, BG, CH, CY, CZ, DE, DK, EE, ES, FI, FR, GB, GR, HR, HU, IE, IS, IT, LT, LU, LV, MC, MK, MT, NL, NO, PL, PT, RO, RS, SE, SI, SK, SM, TR), OAPI (BF, BJ, CF, CG, CI, CM, GA, GN, GQ, GW, KM, ML, MR, NE, SN, TD, TG).

**Published:**

— *with international search report (Art. 21(3))*

(54) **Title:** SYSTEMS AND METHODS OF GRUENEISEN-RELAXATION PHOTOACOUSTIC MICROSCOPY AND PHOTOACOUSTIC WAVEFRONT SHAPING

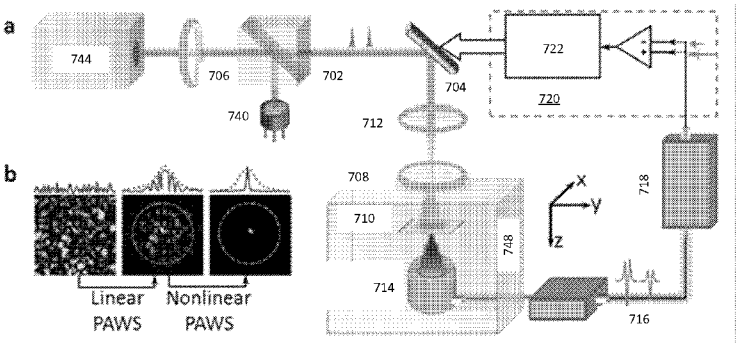


FIG. 7

(57) **Abstract:** Systems and methods for focusing a light pulse within a focus area using nonlinear photoacoustic wavefront shaping (PAWS) are disclosed herein. The method includes modulating a spatial phase pattern of a light pulse's waveform based on a Grueneisen-relaxation photoacoustic (GR-PA) feedback signal. In addition, systems and methods for performing Grueneisen-relaxation photoacoustic microscopy (GR-PAM) are disclosed herein that include analyzing photoacoustic signals resulting from illumination of a focus region by two closely spaced light pulses. A method of obtaining an absorption coefficient of a sample using Grueneisen-relaxation photoacoustic microscopy (GR-PAM) is also disclosed.

WO 2015/077355 A1

# SYSTEMS AND METHODS OF GRUENEISEN-RELAXATION PHOTOACOUSTIC MICROSCOPY AND PHOTOACOUSTIC WAVEFRONT SHAPING

## CROSS REFERENCE TO RELATED APPLICATIONS

[0001] This application is a PCT of U.S. Provisional Application No. 61/906,238 filed on November 19, 2013, which is incorporated herein by reference in its entirety.

## GOVERNMENTAL RIGHTS IN THE INVENTION

[0002] This invention was made with government support under Grant No. R01 CA1 59959 (NIH), R01 CA1 86567 (NIH), DP1 EB01 6986 (NIH), and IS 13 (National Academies Keck Futures Initiative). The government has certain rights in the invention.

## FIELD OF THE INVENTION

[0003] The invention generally relates to systems and methods for improving photoacoustic resolution.

## BACKGROUND OF THE INVENTION

[0004] Confocal microscopy has broad applications in life science, semiconductor inspection, and materials science. It offers better optical resolution and signal-to-background ratio than wide-field microscopy. However, confocal microscopic contrast has been limited to back-scattering and fluorescence; it cannot image non-radiative absorption contrast with sufficient sensitivity.

[0005] Via non-radiative relaxation, excited molecules convert absorbed energy to heat. In biological tissue, almost all endogenous molecules absorb photons at certain wavelengths and generate heat, but only a few produce strong

radiative contrasts, such as fluorescence. Hence, the ability to image non-radiative absorption contrast should extend microscopy to broader applications.

[0006] Recent development of optical-resolution photoacoustic microscopy (OR-PAM) has enabled imaging with absorption contrasts. However, like wide-field optical microscopy, OR-PAM lacks optically defined axial resolution when imaging planar objects—i.e., objects wider than the lateral resolution. The arrival time of the photoacoustic (PA) signal offers depth information, whose resolution is determined by the bandwidth of the ultrasound transducer as limited by the depth of the absorber in tissue. Specifically, the frequency dependence of acoustic attenuation limits the usable ultrasound bandwidth, leading to poor axial resolution. Two-photon absorption has been employed in OR-PAM to achieve better resolution. Yet, it is challenging to effectively separate the two-photon PA signal from the predominant single-photon signal. A transient absorption method was proposed to improve axial resolution. This method relies on the ground state recovery time, which may be applicable to only limited types of molecules. Therefore, there is a need for an imaging system that extends microscopy to imaging a wide variety of non-radiative absorbers with confocal resolution.

## SUMMARY OF THE INVENTION

[0007] In an aspect, the present disclosure provides a method of focusing a light pulse within a focus area using nonlinear photoacoustic wavefront shaping (PAWS) including obtaining an initial GR-PA feedback signal using an initial wavefront from within the focus area; obtaining at least one subsequent GR-PA feedback signal, each subsequent GR-PA feedback signal obtained using a subsequent wavefront determined by altering a preceding wavefront according to a wavefront optimization rule using an immediately preceding GR-PA feedback signal obtained using the preceding wavefront; selecting an optimized wavefront according to an optimization criterion; and focusing the light pulse comprising the optimized wavefront within the focus area at a single-speckle resolution.

[0008] A GR-PA signal is obtained by: delivering a first laser pulse comprising one wavefront to the focus area; detecting a first photoacoustic signal induced by illumination of the focus area by the first laser pulse; delivering a second laser pulse comprising the one wavefront to the focus area at a lag interval time after the delivery of the first laser pulse; detecting a second photoacoustic signal induced by illumination of the focus area by the second laser pulse; and subtracting a first peak-to-peak amplitude of the first photoacoustic signal from a second peak-to-peak amplitude of the second photoacoustic signal to obtain the GR-PA signal. Each subsequent wavefront produces a subsequent GR-PA signal higher than any preceding GR-PA signal. The wavefront optimization rule includes a genetic algorithm. The optimization criterion is chosen from: the optimized wavefront is the wavefront determined after a maximum number of GR-PA signals have been obtained; the optimized wavefront is the wavefront for which a difference in the GR-PA signal associated with the optimized wavefront and the immediately preceding GR-PA signal is less than a minimum GR-PA signal difference; and the optimized wavefront produces a GR-PA signal greater than a minimum threshold GR-PA signal. The maximum number of GR-PA signals ranges from about 100 to about 2000. The optimized wavefront is obtained in an optimization time less than a speckle decorrelation time. The first laser pulse and the second laser pulse include a laser fluence, where the laser fluence may be decreased between obtaining one or more subsequent feedback signals to avoid overheating the sample. The lag interval time is less than about 20 to about 50 μs. Each wavefront includes a spatial phase pattern generated by delivering a laser pulse through a configurable spatial light modulator. The initial wavefront is chosen from a random spatial phase pattern and an optimal spatial phase pattern obtained by a linear photoacoustic wavefront shaping method. The linear photoacoustic wavefront shaping method includes a time-reversed ultrasonically encoded (TRUE) optical focusing method. The optimized GR-PA signal obtained using the optimized waveform is at least 100 times greater than the initial GR-PA signal. The focus

region of the GR-PA signal includes a lateral resolution corresponding to a single speckle. The focus region of the GR-PA signal includes a lateral resolution of less than about 10 μηη. The focus region of the GR-PA signal is centered within an acoustic focus region of an acoustic transducer used to obtain photoacoustic signals. The method may further include centering the focus region within the acoustic focus region by: obtaining a plurality of scanned PA signals using the optimized wavefront scanned across the acoustic focus region at a plurality of scan locations; and using the scan location associated with the highest PA signal of the plurality of scanned PA signals to center the focus region within the acoustic focus region. The optimized wavefront is scanned across the acoustic focus region by applying a linear phase ramp to an optimized spatial phase pattern associated with the optimized wavefront. A high-fluence laser pulse comprising the optimized waveform is delivered to the focus region to perform a laser microsurgery. The laser microsurgery includes a photocoagulation of small blood vessels, a photoablation of tissue, and any combination thereof.

[0009] In another aspect, the present disclosure provides a method of Grueneisen-relaxation photoacoustic microscopy (GR-PAM) of a subject including delivering a first laser pulse to a focus region; detecting a first photoacoustic signal induced by illumination of the focus region by the first laser pulse; after a lag interval time after the delivery of the first laser pulse, delivering a second laser pulse to the focus region; detecting a second photoacoustic signal induced by illumination of the focus region by the second laser pulse; and subtracting a first peak-to-peak magnitude of the first photoacoustic signal from a second peak-to-peak magnitude of the second photoacoustic signal to obtain a GR-PA signal corresponding to the focus region.

[0010] The lag interval time is less than a thermal relaxation time of the subject. The lag interval time is less than about 5 μs to about 20 μs. The first laser pulse heats the focus region from a first temperature to a second temperature, where the first temperature and the second temperature are both within a linear temperature range at which the Grueneisen parameter varies

linearly with respect to temperature. The linear temperature ranges from about 10° C to about 55° C for a biological tissue comprising water, fatty tissues, or any combination thereof. The second temperature is no more than about 5° C higher than the first temperature. The first laser pulse and the second laser pulse each include a pulse width of less than about 5 ns to about 10 ns. The first laser pulse includes a first laser pulse energy and the second laser pulse includes a second laser pulse energy that is essentially equal to the first laser pulse energy. The second laser pulse energy ranges from about 1% to about 100% of the first laser pulse energy. The first laser pulse and the second laser pulse further include a pulse wavelength ranging from about 400 nm to about 1300 nm. The lateral resolution of the GR-PAM is about $1/\sqrt{2}$ times the lateral resolution of OR-PAM performed using similar process parameters. The lateral resolution of the GR-PAM is less than about 0.5 μιτι. The axial resolution of the GR-PAM is at least 10 times finer than the axial resolution of OR-PAM performed using similar process parameters. The axial resolution of the GR-PAM is less than about 5 μιτι. The GR-PAM performs optical sectioning, where an axial FWHM of the GR-PA signal obtained from a planar target is about twice the Rayleigh range of a light beam comprising the first laser pulse and the second laser pulse.

[001 1] In another aspect, the present disclosure provides a method of obtaining an absorption coefficient of a sample using Grueneisen-relaxation photoacoustic microscopy (GR-PAM) including obtaining a plurality of GR-PA signals , each GR-PA signal obtained at a focus region situated at a different penetration depth z within the sample; fitting the plurality of GR-PA signals and associated penetration depths z to a first equation to determine an optical absorption coefficient: APA(z)=Ae ^(-(2p_a z)) where $\Delta PA$ (ζ) is the GR-PA signal at the penetration depth z and A is an amplitude corresponding to the GR-PA signal measured at z = 0; and calculating the optical absorption coefficient from the fitted first equation.

[0012] Each GR-PA signal at each penetration depth z is obtained by: delivering a first laser pulse to the focus region at the penetration depth z;

detecting a first photoacoustic signal induced by illumination of the focus region by the first laser pulse; after a lag interval time after the delivery of the first laser pulse, delivering a second laser pulse to the focus region; detecting a second photoacoustic signal induced by illumination of the focus region by the second laser pulse; and subtracting a first peak-to-peak magnitude of the first photoacoustic signal from a second peak-to-peak magnitude of the second photoacoustic signal to obtain each GR-PA signal. The method may further include determining the concentration of a plurality of molecules in the sample using the obtained absorption coefficient. The plurality of molecules include a known molar extinction spectrum. The plurality of molecules are selected from: oxy-hemoglobin or deoxy-hemoglobin.

## BRIEF DESCRIPTION OF THE DRAWINGS

[001 3] The following figures illustrate various aspects of the disclosure.

[0014] **FIG. 1a** is a fluence distribution for laser pulse 1 ($L_1$). **FIG. 1b** shows a residual temperature rise from laser pulse 1 and fluence distribution of laser pulse 2 ($L_2$). **FIG. 1c** shows a differential pressure rise induced by the Grueneisen-relaxation effect. **FIG. 1d** is a schematic of a GR-PAM system.

[0015] **FIG. 2a** shows a linear relationship between single-pulsed PA amplitude and pulse energy. **FIG. 2b** shows a linear relationship between the increase of the second PA amplitude and the first laser pulse energy. **FIG. 2c** shows the increase of the second PA amplitude versus inter-pulse time delay while both laser pulses had constant energy values.

[0016] **FIG. 3a** summarizes the lateral profiles of a sharp edge measured by OR-PAM and GR-PAM. OR-PAM has a lateral resolution of 0.65 μηη, while GR-PAM has a lateral resolution of 0.41 μιτι. **FIG. 3b** summarizes the lateral profiles of a sharp edge measured by OR-PAM and GR-PAM.

[0017] **FIG. 4a** is a cross-sectional GR-PAM image of red blood cells at a depth of 1.1 μιτι. **FIG. 4b** is a cross-sectional GR-PAM image of red blood cells at a depth of 0 μιτι. **FIG. 4c** is a cross-sectional GR-PAM image of red blood cells at

a depth of -1.1 μηη. **FIG. 4d** is a cross-sectional OR-PAM image of red blood cells at a depth of 1.1 μιτι. **FIG. 4e** is a cross-sectional OR-PAM image of red blood cells at a depth of 0 μιτι. **FIG. 4f** is a cross-sectional OR-PAM image of red blood cells at a depth of -1.1 μιτι. **FIG. 4g** is a side-view GR-PAM image of red blood cells in the *x-z* plane. **FIG. 4h** is a side-view OR-PAM image of the same sample as in **FIG. 4g. FIG. 4i** is a summary of the PA profiles along the dashed lines in **FIG. 4c** and **FIG. 4f.**

[0018] **FIG. 5a** is a schematic diagram of a semi-infinite blood sample. **FIG. 5b** is an OR-PAM cross-sectional image. **FIG. 5c** is a GR-PAM cross-sectional image. **FIG. 5d** is a graph of time-resolved PA signals from the two laser pulses and the differential PA signal when the focus was 60 μιτι below the blood surface. **FIG. 5e** is a graph that shows exponential decay of GR-PA amplitude along depth. **FIG. 5f** is a graph of measured absolute absorption coefficient versus set absorption coefficient.

[0019] **FIG. 6a** is a schematic illustration of the Grueneisen relaxation effect producing a nonlinear photoacoustic signal. **FIG. 6b** is an schematic illustration of the nonlinear PAWS principle.

[0020] **FIG. 7a** is a schematic of the photoacoustic wavefront shaping (PAWS) experimental setup. **FIG. 7b** is an illustration of the two-stage optimization procedure.

[0021] **FIG. 8a** is PA signals before (dashed curve) and after (solid curve) the linear PAWS (Stage 1) optimization. **FIG. 8b** is a graph of the linear improvement factor (defined as the ratio of the PA amplitudes over the initial PA amplitude) versus iteration index.

[0022] **FIG. 9a** shows the initial two PA signals (dashed curve for the first, and solid curve for the second) from the paired laser pulses (separated by 40 μs) in Stage 2, when the phase pattern obtained from the linear PAWS procedure was displayed on the SLM. **FIG. 9b** shows the final two PA signals (dashed curve for the first, and solid curve for the second) after Stage 2 optimization. **FIG. 9c** is a graph of the nonlinear improvement factor (defined by the ratio between the

compensated nonlinear PA amplitudes over the initial value) versus iteration index.

[0023] **FIG. 10a** is a speckle pattern imaged behind a diffuser when a randomized phase pattern was displayed on the SLM. **FIG. 10b** is the optical focus down to a single speckle grain imaged behind a diffuser when the optimized phase pattern from Stage 2 (the inset of **FIG. 9b)** was displayed on the SLM.

[0024] **FIG. 11** is a detailed experimental setup diagram illustrating the OR-PAM/GR-PAM system.

[0025] **FIG. 12a** is a schematic diagram of the experimental setup for transducer calibration. **FIG. 12b** is a graph of the calibrated acoustic sensitivity at the transducer focal plane, with a FWHM of 65$\mu\eta\eta$.

[0026] Corresponding reference characters and labels indicate corresponding elements among the views of the drawings. The headings used in the figures should not be interpreted to limit the scope of the claims.

## DETAILED DESCRIPTION

[0027] Provided herein is a Grueneisen-relaxation photoacoustic microscopy (GR-PAM) based on the Grueneisen- relaxation effect, which extends microscopy to imaging a wide variety of non-radiative absorbers with confocal resolution. GR-PAM sequentially excites an absorber with two almost identical laser pulses. The first laser excitation generates a PA signal and thermally tags the absorber. Owing to the Grueneisen-relaxation effect, the second laser excitation produces a stronger PA signal. GR-PAM detects the amplitude difference between the two PA signal, resulting in confocal performance. GR-PAM images pure absorption contrasts and achieves three-dimensional optical resolution. In addition, GR-PAM can effectively suppress the specular emission in conventional PA signals and probe the interior of a relatively large absorber such as a blood vessel. Taking advantage of the new capabilities of GR-PAM, the absolute optical absorption coefficient without fluence calibration

may be measured, which enables measurements of the concentrations of many endogenous absorbers.

[0028] Scattering of light by wavelength-scale refractive index changes is the reason that media such as paper, frosted glass, fog, and biological tissue appear opaque. The distortion of the optical wavefront propagating within such scattering media makes conventional lens focusing impossible, as the optical wavelets no longer add up in phase at the targeted position. This phenomenon fundamentally limits high-resolution optical imaging techniques, such as microscopy and optical coherence tomography, to depths up to a single transport mean free path (about 1 mm in soft tissue). Invasive procedures, such as embedding optical fibers, are often resorted to when concentrated light is desired beyond this depth, such as in optogenetics and photothermal therapy. When coherent light propagates in a scattering medium, speckles are formed. Despite appearing random, speckles are deterministic within the speckle correlation time. This property has spurred recent advances in optical time-reversal and wavefront-shaping techniques to manipulate the optical wavefront and form a focus within a scattering medium.

[0029] Optical time-reversal focusing is achieved by sensing and phase-conjugating the re-emitted wavefront from an internal "guide star" provided by focused ultrasound (TRUE and TROVE) or embedded fluorescent particles. In contrast, wavefront-shaping focusing is achieved by optimizing the incident wavefront to maximize the signal from a guide star. This pattern can be found using iterative algorithms, or by measuring the so-called "transmission matrix". For absorptive targets, photoacoustic (PA) sensing is promising, as the signal comes directly from the target, as well as being non-harmful and non-invasive.

[0030] So far, focusing by PA-guided wavefront shaping has produced acoustic diffraction-limited spots. The acoustic diffraction limit may be beat and light may be focused to a single optical speckle grain, reaching the optical diffraction limit. The present disclosure provides for a mechanism to obtain a nonlinear PA signal based on the Grueneisen relaxation effect. Using this

nonlinear signal as feedback, PAWS achieves single speckle-grain focusing even when a large number of speckle grains are present within the acoustic focus. A clear optical focus may be obtained on the scale of about 5 to about 7 μιτι, which is about 10 times smaller than the acoustic focus, with a peak fluence ($J/m^2$) enhancement factor of about 6,000.

### I. Grueneisen-relaxation photoacoustic microscopy

[0031] Grueneisen-relaxation photoacoustic microscopy (GR-PAM) obtains images using non-radiative absorption with confocal optical resolution. GR-PAM sequentially delivers two identical laser pulses. The first pulse generates a photoacoustic signal and thermally tags the in-focus absorber. Owing to the Grueneisen-relaxation effect, the second pulse generates a stronger photoacoustic signal from the tagged absorber. GR-PAM detects the amplitude difference between the two co-located photoacoustic signals, resulting in confocal imaging of non-radiative absorption. The optical sectioning with about 2.3 μιτι axial resolution may be improved from about 45 μιτι by conventional acoustic sectioning, and improved the lateral resolution to about 0.41 μιτι by a factor of about 1.6. By suppressing specular emission in conventional photoacoustic signals, GR-PAM enables probing the interior of a relative large optical absorber. This set of new capabilities facilitates the measurement of the absolute absorption coefficient without fluence calibration.

[0032] GR-PAM may be used for high resolution three-dimensional imaging of absorptive contrasts, such as blood vessel, melanoma cells, cell nuclei, lipid, or any other material or contrast agents that absorb light. Conventional photoacoustic microscopy has only acoustic axial resolution. The disclosed technology will enable optical axial resolution, which can be potentially an order of magnitude finer.

[0033] When a short laser pulse excites absorbers under the conditions of both thermal and stress confinements, the initial pressure rise $p_0$ can be written as

$$P_0 = \Gamma_r I_{th} \mu_a F \quad , \qquad (1)$$

where $\Gamma$ is the Grueneisen parameter, $\eta_{th}$ is the heat conversion efficiency, $\mu_a$ is the optical absorption coefficient, and $F$ is the optical fluence. The Grueneisen parameter $\Gamma$ depends on the local temperature. When the temperature variation is within a few degrees, the dependence can be estimated as a linear function of temperature.

[0034] In GR-PAM, two identical nanosecond laser pulses are sequentially delivered within a sub-microsecond delay. According to Eq. 1, the first pulse generates an initial pressure rise $p_{01}$:

$$p_{01} = \Gamma_0 \eta_{th} \mu_a F \quad , (2)$$

where $\Gamma_0$ is the Grueneisen parameter at the baseline temperature.

[0035] The temperature rise at the focus responsible for the initial pressure rise also alters the local Grueneisen parameter within the thermal relaxation time. This phenomenon is the Grueneisen-relaxation effect. Note that the Grueneisen-relaxation time is usually orders-of-magnitude longer than the stress-relaxation time.

[0036] Within the Grueneisen-relaxation time, the same absorber may be excited with the second laser pulse, which generates another initial pressure rise $p_{02}$:

$$p_{02} = (\Gamma_0 + b\eta_{th} \mu_a F)\eta_{th} \mu_a F \quad , \qquad (3)$$

where $b$ is a coefficient that relates the thermal energy absorbed from the first pulse to the Grueneisen parameter change. Note that $b$ varies with the time delay between the two laser pulses.

[0037] If the optical fluence follows 2D Gaussian distributions in the lateral directions, at a certain axial position, the fluence can be written as

$$F\{x,y) = -\frac{E}{\pi w^2}\exp(-\frac{x^2 + y^2}{w^2}) \quad , \quad (4)$$

where $E$ is the pulse energy at the absorber plane, $x$ and $y$ are the coordinates in the lateral directions, and $w$ is the dimension of the waist of the Gaussian beam at the current axial position.

[0038] Because the optical focal spot is well confined within the acoustic voxel, the detected PA amplitude is proportional to the total initial pressure rise in an acoustic detection voxel. Therefore, the PA amplitude induced by the first laser pulse can be derived from the spatial integration of $P_m$:

$$PA, = k\Gamma_0\eta_{th}E \iint \mu_\alpha(x,y)\frac{1}{\pi w^2}\exp(-\frac{x^2 + y^2}{w^2})dxdy \quad , \quad (5)$$

where $k$ is a constant related to the PA detection sensitivity.

[0039] Similarly, the PA amplitude induced by the second laser pulse can be written as

$$PA_2 = k\Gamma_0\eta_{th}E\iint \mu_a(x,y)\frac{1}{\pi w^2}\exp(-\frac{x^2 + y^2}{w^2})dxdy + kb\eta_{th}^2E^2\iint \mu_a^2(x,y)\frac{1}{\pi^2 w^4}\exp(-\frac{x^2 + y^2}{w^2/2})dxdy \quad . \quad (6)$$

The right-hand side of Eq. 6 has two parts. The first part is the same as $PA_1$. The second part is generated from the joint effect of the first pulse's Grueneisen relaxation and the second pulse's excitation.

[0040] Subtracting Eq. 5 from Eq. 6 obtains the differential signal between $PA_2$ and $PA_1$, called the GR-PA signal:

$$\Delta PA = PA_2 - PA_1 = kbri_{th}^2E^2 \iint \mu_\alpha^2(x,y)\frac{1}{\pi^2 w^4}\exp(-\frac{x^2 + y^2}{w^2/2})dxdy \quad . \quad (7)$$

[0041] For a planar target with a constant $\mu_a$, the GR-PA signal becomes

$$APA = kb\eta_{th}^2\mu_a^2E^2\frac{1}{2\pi w^2} . \quad (8)$$

The Gaussian beam waist varies with the distance $z$ from the focus in a relationship of

$$w^2 = w_0^2(1+z^2/z_R^2) , \quad (9)$$

where $w_0$ is the beam waist at the focus, and $z_R$ is the Rayleigh range. When $z = z_R$, the GR-PA signal amplitude decreases by half of that when the beam is focused at the absorber plane. Hence the axial full width at half maximum (FWHM) of a planar target is twice the optical Rayleigh range, giving GR-PAM optical sectioning capability.

[0042] In comparison, the OR-PAM signal amplitude from a planar target is

$$pA = k\Gamma_0\eta_\Lambda\mu_\alpha E . \quad (10)$$

Since none of the parameters on the right-hand side of Eq. 10 change with the focal distance, conventional OR-PAM cannot provide optical sectioning for planar targets.

[0043] The lateral resolution of GR-PAM is estimated from a point target. When scanning the point target in the *x*-*y* plane, GR-PAM generates a two-dimensional image, expressed by

$$\Delta PA(x,y) = kb\eta_{th}^2\mu_a^2E^2\frac{1}{\pi^2w^4}\exp(-\frac{x^2+y^2}{w^2/2}) . \quad (11)$$

The point spread function of the GR-PAM follows a Gaussian distribution with a waist of $w/\sqrt{2}$.

[0044] In comparison, OR-PAM gives an image described by

$$PA_1(x,y) = k\Gamma_0\eta_{th}\mu_\alpha E\frac{1}{\pi w^2}\exp(-\frac{x^2+y^2}{w^2}) \quad . (12)$$

The point spread function of OR-PAM follows a Gaussian distribution with a waist dimension of $w$. Therefore, the lateral resolution of GR-PAM is better than that of OR-PAM by a factor of $\sqrt{2}$.

[0045] GR-PAM is analogous to conventional confocal microscopy. In GR-PAM, the first laser pulse thermally tags absorbers. Since the fluence in the optical focus zone is much higher than that out of the focal zone, only absorbers within the focal zone can be effectively tagged. The second laser pulse excites the same absorbers. The Grueneisen-relaxation effect allows the two temporally separated but spatially co-located laser pulses to jointly act on the same absorbers and produce an increased signal. The differential operation rejects the non-tagged PA signals, analogous to the pinhole in optical confocal microscopy. Typical optical fluence distributions, the residual temperature rise, and a differential pressure distribution are illustrated in **FIG. 1a, FIG. 1b** and **FIG. 1c.**

[0046] **FIG. 1d** is a schematic of a GR-PAM system. In an aspect, the GR-PAM system may include an amplifier **102,** a high-speed digitizer **104;** a computer **106;** photodiodes 1 and 2 **108, 110;** and a parabolic mirror **112.** In an aspect, the amplifier may be an about 40-dB broadband amplifier. In another aspect, *p*oi may be the initial pressure from the first laser pulse, **P02** may be the initial pressure from the second laser pulse, and $\Delta\rho_0$ = **Po2 - Poi -** Two identical pulsed lasers **114, 116** may be sequentially triggered with a sub-microsecond delay. In an aspect, the lasers may have an about 532 nm wavelength, about 1 ns pulse duration, and a SPOT of about 100-200-532. A subpanel in **FIG. 1d** shows the temporal relationship among the laser triggers and the PA signals. The laser energy is calibrated by two photodiodes. The two laser beams are spatially aligned and coupled into a single-mode fiber connected to a PA probe. The PA probe may employ an objective **118** to focus the laser beam. In an

aspect, the objective may be a 0.63 numerical aperture (NA) objective, where 0.63 NA is the highest for reflection-mode OR-PAM. A parabolic mirror **112** with a center opening may transmit light and reflect the ultrasonic wave to a custom-made ultrasound transducer **120.** The optical objective and the parabolic mirror may focus to the same spot to optimize the PA detection sensitivity. In an aspect, the output of the ultrasound transducer may be amplified by 40 dB, digitized at 500 MHz, and recorded in a PC. At each position, two PA signals are recorded. The PC and a FPGA card may control a three-axis motorized to perform three-dimensional scanning.

[0047] In an aspect, a method of Grueneisen-relaxation photoacoustic microscopy (GR-PAM) of a subject may include delivering a first laser pulse to a focus region; detecting a first photoacoustic signal induced by illumination of the focus region by the first laser pulse; after a lag interval time after the delivery of the first laser pulse, delivering a second laser pulse to the focus region; detecting a second photoacoustic signal induced by illumination of the focus region by the second laser pulse; and subtracting a first peak-to-peak magnitude of the first photoacoustic signal from a second peak-to-peak magnitude of the second photoacoustic signal to obtain a GR-PA signal corresponding to the focus region.

[0048] In an aspect, the lag interval time may be less than a thermal relaxation time of the subject. In another aspect, the lag interval time may range from less than about 0.1 μs to less than about 50 μs. In various aspects, the lag interval time may range from less than about 0.1 μs to less than about 0.5 μs, from less than about 0.3 μs to less than about 1 μs, from less than about 0.5 μs to less than about 2 μs, from less than about 1 μs to less than about 5 μs, from less than about 2 μs to less than about 10 μs, from less than about 5 μs to less than about 15 μs, from less than about 10 μs to less than about 20 μs, from less than about 15 μs to less than about 25 μs, from less than about 20 μs to less than about 30 μs, from less than about 25 μs to less than about 35 μs, from less than about 30 μs to less than about 40 μs, from less than about 35 μs to less

than about 45 μs, and from less than about 40 μs to less than about 50 μs. In one aspect, the lag interval time may be 0.5 μs.

[0049] The first laser pulse may heat the focus region from a first temperature to a second temperature, where the first temperature and the second temperature are both within a linear temperature range at which the Grueneisen parameter varies linearly with respect to temperature. In an aspect, the linear temperature range may range from about 10°C to about 55°C for a biological tissue comprising water, fatty tissues, or any combination thereof. In various aspects, the linear temperature range may range from about 10 °C to about 20 °C, from about 15 °C to about 25 °C, from about 20 °C to about 30 °C, from about 35 °C to about 45 °C, from about 40 °C to about 50 °C, and from about 45 °C to about 55 °C. In an aspect, the second temperature may be no more than about 5° C higher than the first temperature.

[0050] The first laser pulse and the second laser pulse may each include a pulse width of less than about 5 ns to less than about 20 ns. In various aspects, the pulse width may range from about 5 ns to about 7 ns, from about 6 ns to about 8 ns, from about 7 ns to about 9 ns, from about 8 ns to about 10 ns, from about 10 ns to about 15 ns, from about 12 ns to about 17 ns, and from about 15 ns to about 20 ns. In one aspect, the pulse width may be 10 ns.

[0051] The first laser pulse includes a first laser pulse energy and the second laser pulse includes a second laser pulse energy that is essentially equal to the first laser pulse energy. The second laser pulse energy ranges from about 1% to about 100% of the first laser pulse energy. In various aspects, the second laser pulse energy may range from about 1% to about 20%, from about 10% to about 30%, from about 20% to about 40%, from about 30% to about 50%, from about 40% to about 60%, from about 50% to about 70%, from about 60% to about 80%, from about 70% to about 90%, and from about 80% to about 100% of the first laser pulse energy. The first laser pulse and the second laser pulse may further include a pulse wavelength ranging from about 400 nm to about 1300 nm. In various aspects, the first and second laser pulses may have a wavelength

ranging from about 400 nm to about 600 nm, from about 500 nm to about 700 nm, from about 600 nm to about 800 nm, from about 700 nm to about 900 nm, from about 800 nm to about 1000 nm, from about 900 nm to about 1100 nm, from about 1000 nm to about 1200 nm, and from about 1100 to about 1300 nm.

[0052] The lateral resolution of the GR-PAM may be about 1/V2 times the lateral resolution of OR-PAM performed using similar process parameters. In an aspect, the lateral resolution of the GR-PAM may be less than about 0.5 μιτι. In another aspect, the axial resolution of the GR-PAM may be at least 10 times finer than the axial resolution of OR-PAM performed using similar process parameters. In one aspect, the axial resolution of the GR-PAM may be less than about 5 μιτι. The GR-PAM may perform optical sectioning, where an axial FWHM of the GR-PA signal obtained from a planar target may be about twice the Rayleigh range of a light beam comprising the first laser pulse and the second laser pulse.

[0053] In another aspect, a method of obtaining an absorption coefficient of a sample using Grueneisen-relaxation photoacoustic microscopy (GR-PAM) may include obtaining a plurality of GR-PA signals , each GR-PA signal obtained at a focus region situated at a different penetration depth z within the sample; fitting the plurality of GR-PA signals and associated penetration depths z to a first equation to determine an optical absorption coefficient:

$$\Delta PA(z) = Ae^{-(2\mu_a z)}; \quad (13)$$

where ΔPA (ζ) is the GR-PA signal at the penetration depth z and A is an amplitude corresponding to the GR-PA signal measured at z = 0; and calculating the optical absorption coefficient from the fitted first equation.

[0054] Each GR-PA signal at each penetration depth z may be obtained by delivering a first laser pulse to the focus region at the penetration depth z; detecting a first photoacoustic signal induced by illumination of the focus region by the first laser pulse; after a lag interval time after the delivery of the first laser

pulse, delivering a second laser pulse to the focus region; detecting a second photoacoustic signal induced by illumination of the focus region by the second laser pulse; and subtracting a first peak-to-peak magnitude of the first photoacoustic signal from a second peak-to-peak magnitude of the second photoacoustic signal to obtain each GR-PA signal. The method may further include determining the concentration of a plurality of molecules in the sample using the obtained absorption coefficient. In an aspect, the plurality of molecules may include a known molar extinction spectrum. The plurality of molecules may include but is not limited to oxy-hemoglobin or deoxy-hemoglobin.

[0055] Non-radiative relaxation is a primary energy conversion mechanism. The Grueneisen-relaxation effect, as a natural result of non-radiative relaxation, exists in most light-matter interactions. A photoacoustic signal is inherently sensitive to local Grueneisen parameter. The combination of the Grueneisen-relaxation effect and photoacoustic detection enables high-resolution label-free imaging of many endogenous absorbers, such as hemoglobin, lipid, melanin, DNA/RNA, protein, or water. Although the specificity of single-wavelength label-free imaging might not be as high as a fluorescence-labeled counterpart, multiple wavelengths may be used to spectrally separate primary absorbers. Functional parameters associated with these absorbers, e.g., the oxygen saturation of blood, can be mapped in 3D with high resolution.

[0056] GR-PAM requires a pulse energy similar to that of conventional OR-PAM. Since the differential PA signal amplitude is proportional to the residual temperature, a good PA signal from the first laser pulse ensures effective thermal tagging. However, the differential operation in GR-PAM decreases the signal-to-noise ratio (SNR). Modulated thermal tagging may be used to improve SNR. Averaging or more sensitive ultrasound detection may improve SNR in one aspect. In terms of light exposure, the average laser power of GR-PAM may be twice as high as that in OR-PAM due to the second laser pulse. If cumulative heating starts to approach the damage threshold, the laser pulse energy can be reduced at the expense of SNR. Unlike conventional OR-PAM, the GR-PAM

signal is proportional to the square of the optical absorption coefficient. Thus the square root of the GR-PA signal may be used if a linear mapping of the absorption coefficient is desired.

[0057] Using a dual-pulse laser system and a high-NA PA probe, GR-PAM improves the axial resolution from the acoustic scale to the optical focal depth, and the lateral resolution was improved by ~V2. The dual-laser system can be further simplified by splitting a single laser beam into two and delaying one of them. The point-by-point depth scanning prolongs data acquisition, which might be mitigated by increasing the laser repetition rate and the scanning speed.

[0058] Besides its improved resolution, GR-PAM enables probing the interior properties of a relatively large absorber. While specular emission limits conventional PA detection to the surface of the absorber, GR-PAM thermally tags inner parts of the absorber and suppresses the specular emission. Via scanning the focus, the signal decay constant can be measured to quantify the absolute absorption coefficient without fluence calibration. The absorption contrast, the three-dimensional optical resolution, and the unique capability to probe the interior of absorbers may extend microscopy to broader applications.

## II. Nonlinear photoacoustic wavefront shaping (PAWS) for single speckle-grain optical focusing in scattering media

[0059] Non-invasively focusing light into strongly scattering media, such as biological tissue, is highly desirable but challenging. Recently, wavefront-shaping technologies guided by ultrasonic encoding or photoacoustic sensing have been developed to address this limitation. So far, these methods provide only acoustic diffraction-limited optical focusing. Here, nonlinear photoacoustic wavefront shaping (PAWS) achieves optical diffraction-limited (i.e., single-speckle-grain sized) focusing in scattering media. A dual-pulse excitation approach generates nonlinear photoacoustic (PA) signals based on the Grueneisen relaxation effect. These nonlinear PA signals may be used as feedback to guide iterative wavefront optimization. By maximizing the amplitude of the nonlinear PA signal,

light is effectively focused to a single optical speckle grain within the acoustic focus. A clear optical focus may be on the scale of about 5 to about 7 μιτι, which is about 10 times smaller than the acoustic focus, with an enhancement factor of about 6,000 in peak fluence.

[0060] The PAWS system setup is illustrated schematically in **FIG. 7a** in an aspect. The system may include a polarized beam splitter (PBS) **702,** a spatial light modulator (SLM) **704,** a half-wave plate (λ/2) **706.** The scattering medium consists of a ground glass diffuser **708** and a layer of optically absorbing whole blood **710.** The incident light reflected from the SLM surface may be scattered by a diffuser **708,** generating a random speckle pattern with about 5-μιτι speckle grains on the blood layer **710.** The system may further include a lens **712,** an ultrasonic transducer **714,** an amplifier **716,** an oscilloscope **718,** and a computer **720** with a genetic algorithm **722.** The whole blood **710** and the ultrasound transducer **714** may be within water **724.**

[0061] In an aspect, a method of focusing a light pulse within a focus area using nonlinear photoacoustic wavefront shaping (PAWS) may include obtaining an initial GR-PA feedback signal using an initial wavefront from within the focus area; obtaining at least one subsequent GR-PA feedback signal; selecting an optimized wavefront according to an optimization criterion; and focusing the light pulse comprising the optimized wavefront within the focus area at a single-speckle resolution. Each subsequent GR-PA feedback signal may be obtained using a subsequent wavefront determined by altering a preceding wavefront according to a wavefront optimization rule using an immediately preceding GR-PA feedback signal obtained using the preceding wavefront

[0062] In an aspect, a GR-PA signal may be obtained by: delivering a first laser pulse comprising one wavefront to the focus area; detecting a first photoacoustic signal induced by illumination of the focus area by the first laser pulse; delivering a second laser pulse comprising the one wavefront to the focus area at a lag interval time after the delivery of the first laser pulse; detecting a second photoacoustic signal induced by illumination of the focus area by the

second laser pulse; and subtracting a first peak-to-peak amplitude of the first photoacoustic signal from a second peak-to-peak amplitude of the second photoacoustic signal to obtain the GR-PA signal. Each subsequent wavefront may produce a subsequent GR-PA signal higher than any preceding GR-PA signal. In an aspect, the wavefront optimization rule may include a genetic algorithm. The optimization criterion may include, but is not limited to the optimized wavefront is the wavefront determined after a maximum number of GR-PA signals have been obtained; the optimized wavefront is the wavefront for which a difference a GR-PA signal associated with the optimized wavefront and the immediately preceding GR-PA signal is less than a minimum GR-PA signal difference; and the optimized wavefront produces a GR-PA signal greater than a minimum threshold GR-PA signal.

[0063] In an aspect, the maximum number of GR-PA signals ranges from about 100 to about 2000. In various aspects, the maximum number of GR-PA signals may range from about 100 to about 500, from about 250 to about 750, from about 500 to about 1000, from about 750 to about 1250, from about 1000 to about 1500, from about 1250 to about 1750, and from about 1500 to about 2000. In an aspect, the optimized wavefront may be obtained in an optimization time less than a speckle decorrelation time. The first laser pulse and the second laser pulse may include a laser fluence, where the laser fluence may be decreased between obtaining one or more subsequent feedback signals to avoid overheating the sample. The lag interval time may be less than about 0.1 μs to less than about 50 μs. In various aspects, the lag interval time may range from less than about 0.1 μs to less than about 0.5 μs, from less than about 0.3 μs to less than about 1 μs, from less than about 0.5 μs to less than about 2 μs, from less than about 1 μs to less than about 5 μs, from less than about 2 μs to less than about 10 μs, from less than about 5 μs to less than about 15 μs, from less than about 10 μs to less than about 20 μs, from less than about 15 μs to less than about 25 μs, from less than about 20 μs to less than about 30 μs, from less than about 25 μs to less than about 35 μs, from less than about 30 μs to less

than about 40 μs, from less than about 35 μs to less than about 45 μs, and from less than about 40 μs to less than about 50 μs. In one aspect, the lag interval time may be 20 μs.

[0064] Each wavefront may include a spatial phase pattern generated by delivering a laser pulse through a configurable spatial light modulator. In an aspect, the initial wavefront may be chosen from a random spatial phase pattern and an optimal spatial phase pattern obtained by a linear photoacoustic wavefront shaping method. The linear photoacoustic wavefront shaping method may include a time-reversed ultrasonically encoded (TRUE) optical focusing method. In an aspect, the optimized GR-PA signal obtained using the optimized waveform may be at least 100 times greater than the initial GR-PA signal.

[0065] In an aspect, the focus region of the GR-PA signal may include a lateral resolution corresponding to a single speckle. The focus region of the GR-PA signal may include a lateral resolution of less than about 10 μιτι. In various aspects, the lateral resolution may range from less than about 0.5 μιτι to less than about 2 μιτι, from less than about 1 μιτι to less than about 5 μιτι, from less than about 3 μιτι to less than about 6 μιτι, from less than about 5 μιτι to less than about 8 μιτι, and from less than about 7 μιτι to less than about 10 μιτι. The focus region of the GR-PA signal may be centered within an acoustic focus region of an acoustic transducer used to obtain photoacoustic signals.

[0066] In an aspect, the method may further include centering the focus region within the acoustic focus region by obtaining a plurality of scanned PA signals using the optimized wavefront scanned across the acoustic focus region at a plurality of scan locations and using the scan location associated with the highest PA signal of the plurality of scanned PA signals to center the focus region within the acoustic focus region. The optimized wavefront may be scanned across the acoustic focus region by applying a linear phase ramp to an optimized spatial phase pattern associated with the optimized wavefront. In an aspect, a high-fluence laser pulse including the optimized waveform may be delivered to the focus region to perform a laser microsurgery. The laser microsurgery may

include a photocoagulation of small blood vessels, a photoablation of tissue, and any combination thereof.

[0067] The PA effect describes the formation of acoustic waves due to absorption of light, which is usually short-pulsed. The PA amplitude is proportional to the product of the absorbed optical energy density and the local Grueneisen parameter. It is well known that the Grueneisen parameters of many materials are highly temperature dependent. For example, from about **20°C** to about **40°C,** the Grueneisen parameter of water or diluted aqueous solutions may increase by about 96%. Within the thermal confinement time, the temperature rise due to the absorption of light lingers and changes the local Grueneisen parameter accordingly, which is referred to as the Grueneisen relaxation effect.

[0068] A dual-pulse excitation approach is used to obtain a nonlinear PA signal based on the Grueneisen relaxation effect. As shown in **FIG. 6a,** two identical laser pulses are fired sequentially to excite the same absorber. Two laser pulses with equal energy E are incident on an optical absorber. The first pulse causes a sustained change in the Grueneisen parameter—referred to as the Grueneisen relaxation effect—due to an increase in temperature. Within the thermal confinement time, the change in the Grueneisen parameter $\Delta\Gamma$ causes the amplitude from the second PA signal ($V_2$) to be stronger than that from the first **(Vi).** The difference between the peak-to-peak amplitudes AV is nonlinear—proportional to the square of the laser pulse energy. At the first laser pulse, the Grueneisen parameter is determined by the initial temperature. At the second laser pulse, the Grueneisen parameter is changed (usually increased) due to the Grueneisen relaxation effect. Therefore, the second PA signal has a different amplitude from the first one. If the PA amplitude is assumed to be proportional to the laser energy and the Grueneisen parameter is assumed to be linearly dependent on the local temperature, the amplitude difference between the two PA signals is proportional to the square of the laser energy (or fluence). A detailed derivation is shown as follows.

[0069] The peak-to-peak amplitude of the first PA signal is given by the following integral:

$$V_1 = k\iint A(x, y)T^{\wedge}{}_{a}F(x, y)dxdy\,, \qquad (16)$$

[0070] where $k$ is a constant coefficient, $A(x, y)$ is the normalized acoustic detection sensitivity, $\Gamma_0$ is the Grueneisen parameter at the initial temperature $T_0$, $\mu_\alpha$ is the material absorption coefficient, and $F(x,y)$ is the optical fluence distribution. As defined herein below, all PA amplitudes refer to peak-to-peak values. Within the acoustic resolution voxel, both $\Gamma_0$ and $\mu_\alpha$ are assumed to be uniform and constant, and the integration along the z-axis direction is taken into account in the constant coefficient $k$. $A(x, y)$ is frequently approximated using a Gaussian function, $A(x, y) = \frac{1}{2\pi\sigma^2}\exp(-\frac{x^2+y^2}{2\sigma^2})$, where $2\sqrt{\ln 2}\sigma$ is the full width at half maximum (FWHM) of the one-way transducer response.

[0071] The Grueneisen parameter immediately before the second laser pulse can be approximated as

$$\Gamma = \Gamma_0 + \eta\Gamma_0'\mu_a F\,, \qquad (17)$$

[0072] where $\eta$ is a constant coefficient that converts absorbed optical energy density into temperature rise, and $\Gamma_0'$ is the first-order derivative of the Grueneisen parameter with respect to temperature at $T_0$. Therefore, the amplitude of the second PA signal is

$$V_2 = k\iint A(x, y)[\Gamma_0 + \eta\Gamma_0'\mu_\alpha F(\chi, y)]\mu_a F(x, y)dxdy\,. \qquad (18)$$

[0073] The amplitude difference between the two PA signals is

$$\Delta V = V_2 - V_1 = k\eta\Gamma_0'\mu_a^2\iint A(x,y)F^2(x, y)dxdy\,. \qquad (19)$$

[0074] This amplitude difference $AV$ is proportional to the square of the optical fluence, thus termed the nonlinear PA amplitude.

[0075] When the amplitude from a single PA signal is used as feedback to iterative wavefront shaping (linear PAWS), optical energy is concentrated into the acoustic focus. To focus light to the optical diffraction limit, the nonlinear PA amplitude $AV$ can be used as feedback (nonlinear PAWS). The reason for the narrower optical focus can be explained by rewriting equation (19) as

$$AV = k\eta\Gamma_0'\mu_a^2(\overline{F}^2 + F_{Var}), \quad (20)$$

[0076] where $\overline{F} = \iint A(x,y)F(x,y)dxdy$ and $F_{Var} = \iint A(x,y)[F(x,y) - \overline{F}]^2 dxdy$ can be treated as the mean and variance of $F(x,y)$, with a probability density function of $A(x,y)$. Since both $\overline{F}^2$ and $F_{Var}$ are non-negative, $AV$ is maximized when both $\overline{F}^2$ and $F_{Var}$ are maximized. $\overline{F}^2$ is proportional to $V_1^2$ and therefore reaches its maximum when light is concentrated within the acoustic focus. Maximizing $F_{Var}$ is the same as maximizing the uniqueness of $F(x,y)$. Therefore, if the total optical energy is constrained, $F_{Var}$ is maximized when all the optical energy is focused to a single speckle grain with nonlinear PAWS.

[0077] **FIG. 6b** further explains why nonlinear PAWS can focus light to a single speckle grain using an idealized example. When the same optical energy is concentrated to fewer speckle grains within an ultrasound focus, linear PA amplitude does not increase significantly, but nonlinear PA amplitude approximately increases inversely proportionally with the number of bright speckle grains. Therefore, by maximizing AV, light can be focused as tightly as the optical diffraction limit (i.e., one speckle grain). The blue dashed circles represent the ultrasonic focal region. The ultrasonic detection sensitivity may be

simplified to be relatively uniform within a circular focal area, and assumed that the total light energy is constant and evenly distributed among the speckle grains within the ultrasonic focus. Consider two different speckle patterns i and j: speckle pattern i has multiple speckle grains within the ultrasonic focus; speckle pattern j has only one speckle grain. In speckle pattern i, linear PAWS maximizes total energy inside acoustic focus, and in speckle pattern j, nonlinear PAWS maximizes peak energy density inside acoustic focus. In these two cases, the two linear PA amplitudes $V_1$, and $V_{ij}$ are the same, but the two nonlinear PA amplitudes $V_i$, and $V_j$ are significantly different. Compared with speckle pattern i, speckle pattern j concentrates light onto a smaller area and thus causes a higher temperature rise, resulting in a stronger nonlinear PA signal. If all speckle grains have the same area, from equation (19), the nonlinear PA amplitude can be simplified as

$$\Delta V = \frac{1}{M} k\eta\Gamma_0 \mu_a^2 A_0 \frac{E^2}{s^2}, \qquad (21)$$

[0078] where $M$ is the number of speckle grains within the acoustic focus, $A_0$ is the constant acoustic detection sensitivity, $E$ is the total pulse energy, and s is the area of one speckle grain. Equation (21) shows that the nonlinear PA amplitude $A_V$ increases inversely with $M$, and is maximized when $M$ = 1 (optical diffraction-limited focusing). The fluence ($\frac{E}{Ms}$) is also inversely proportional to $M$. Thus the nonlinear PA amplitude is proportional to the fluence at constant incident laser energy. Although this conclusion is based on idealized assumptions, it is helpful for estimating the order of magnitude of the peak fluence.

[0079] To date, optical focusing using PA-guided wavefront shaping has been limited by acoustic diffraction when extended absorbers are targeted. To break through the acoustic resolution limit, nonlinear PAWS has been proposed and demonstrated. Using dual-pulse excitation, nonlinear PA signals were generated based on the Grueneisen relaxation effect. By maximizing the

nonlinear PA amplitude, diffused light was able to be focused into a single optical mode. The focus may be about **5.1** μιτι χ about **7.1** μιτι laterally, about an order of magnitude smaller than the acoustic focal size in each dimension. Note that, about **169** speckle grains exist within the acoustic focal region (determined by taking the ratio between the area of the acoustic focus and the area of a single speckle grain), but after nonlinear PAWS, only one was dominant within the final optical focus. While the absorber may be positioned behind a ground glass diffuser, the same principles may be applied when focusing to absorbers within scattering media, as long as the media are transparent to ultrasound.

[0080] The peak fluence enhancement was estimated to be about **6000** times (about **60** times from the linear PAWS stage and about **100** times from the nonlinear PAWS stage). The peak fluence enhancement can also be estimated from the temperature rise. At the end the nonlinear PAWS, the second PA amplitude $\mathbf{V_2}$ was about **168%** greater than the first PA amplitude **Vi,** which was measured at room temperature of about **20°C (FIG. 9b).** Assuming that the Grueneisen parameter is proportional to the temperature rise, the corresponding temperature rise is estimated to be about 34°C. From here, the final fluence *F* is predicted as

$$F = \frac{ATpC_v}{\mu_a} = \frac{34K \times lg\text{-}cm^{-3} \times 4000mJ \cdot g^{-1} \cdot K^{-1}}{240cm^{-1}} = 5blmJ\text{-}cm^{-2}, \quad \textbf{(22)}$$

[0081] where p is the mass density of blood, $Cv$ is the heat capacitance of blood, and $\mu_a$ is the absorption coefficient of blood. Compared to the initial fluence of about **0.1** mJ-cm$^{-2}$, the final peak fluence is increased by about **5670** times, which agrees with the aforementioned estimation of about **6000** times.

[0082] To date, there has been only one other demonstration of noninvasive speckle-scale optical focusing inside scattering media, by using time reversal of variance-encoded light (TROVE). In TROVE, the scattered light from the scattering medium is recorded at four different positions, and a focused ultrasound beam is used to define the target region. Speckle-scale focusing is then obtained by computing the appropriate phase map from the measured

speckle fields. Despite achieving similar goals, TROVE and nonlinear PAWS are complementary: TROVE time-reverses ultrasonically encoded light, and is therefore more applicable for non- or low-absorption targets. In comparison, nonlinear PAWS is preferred in applications with absorptive targets, such as blood vessels or melanomas in biological tissue. Furthermore, the peak enhancement reported in TROVE is about 110-fold, whereas, PAWS demonstrated an unprecedented peak enhancement of about 6,000-fold, which is a significant advantage in many applications, such as photothermal therapy or optogenetic excitation, that desire intense focusing.

[0083] In an aspect, the optimization speed may be increased. Linear and nonlinear PAWS may take several hours in total. To maintain the deterministic property of the scattering medium, the PAWS focusing procedure must be completed within the speckle correlation time, which is on the order of one millisecond for *in vivo* tissue. Although the SLM operates at 60 Hz, it may take about 1.2 s for the SLM display to fully stabilize. Due to this long optimization time, stable diffusers may be used. In various aspects, faster devices may be used to improve the speed of optimization. For example, digital mirror devices with switching times of about 22 μs have been used in wavefront shaping, and may shorten the optimization. The speed may also affect the choice in the number of controlled blocks used on the SLM. On one hand, the optimization time with the genetic algorithm scales linearly with the number of blocks. On the other hand, the potential peak enhancement also increases linearly. In an aspect, about 192 × 108 may be used as a practical compromise.

[0084] The generation of nonlinear PA signal requires only a reasonable temperature rise. An initial fluence of about 6 mJ-cm$^{-2}$ may be used for nonlinear PAWS, which is well below the ANSI safety limit of 20 mJ-cm$^{-2}$. To avoid potential thermal damage, the laser energy may be attenuated during nonlinear optimization. Since nonlinear PAWS successfully proceeded with fluence as low as about 6 mJ-cm$^{-2}$, the laser energy may be further reduced if safety was a concern in future applications. On the other hand, the high optical fluence after

nonlinear PAWS could potentially be leveraged for laser microsurgery at optical resolution in deep tissue, including photocoagulation of small blood vessels and photoablation of tissue. Without invasive probes, laser microsurgery is limited to depths of several hundred micrometers. Nonlinear PAWS could extend the operating depths, while maintaining single speckle grain focusing. This type of microsurgery could potentially lead to new minimally invasive or noninvasive treatment of Parkinson's disease or epilepsy.

[0085] The nonlinear PA signal is assumed to be quadratic with the laser pulse energy, based on the linear temperature dependence of the Grueneisen parameter. However, even in the presence of higher-order temperature dependence of the Grueneisen parameter, nonlinear PAWS can still lead to optical diffraction-limited focusing. It should also be noted that the optical focal spot produced using nonlinear PAWS should be near the center of the acoustic focus. However, the precision is limited by the signal-to-noise ratio of the final PA signals and the exact acoustic focal profile.

[0086] The expected peak improvement factor for phase-only wavefront-shaping is given by

$$\text{Factor} = \pi / 4[(N - 1) / M] + 1, \qquad (23)$$

[0087] where $N$ is the number of independently controlled SLM blocks and $M$ is the number of optical speckle grains within the acoustic focus. In an aspect, the number of independently controlled SLM blocks may be about 192x1 08. In another aspect, the number of optical speckle grains within the acoustic focus may be about 169 in the linear PAWS stage. Thus, the theoretical enhancement ratio from the linear PAWS may be about 97. In an aspect, the enhancement may be about 60 **(FIG.** 7b). In Stage 1, linear PAWS focuses light into the acoustic focal region. In Stage 2, nonlinear PAWS focuses light onto a single-speckle grain. The dashed circles represent the acoustic focal region. A typical intensity distribution (green solid line) is shown above the speckle illustrations. The blue dotted envelopes represent the acoustic sensitivity. The difference could be due to the laser-mode fluctuation, non-uniformity of optical illumination

on the SLM, stray light, mechanical instability of the system, and measurement errors. Nonetheless, after linear PAWS, the optical fluence within the acoustic focus was sufficient to generate detectable nonlinear PA signals. After nonlinear PAWS, the number of bright speckle grains would ideally reduce from about 169 to 1. Hence, an improvement factor of about 169 may be expected after nonlinear PAWS. In one aspect, the improvement may be about 100 **(FIG. 9c).** **FIG. 10a** and **FIG. 10b** summarize the visualization of single speckle grain focusing using nonlinear PAWS. The peak fluence enhancement of about 6,000 is also approximately consistent with the expected improvement factor from equation (23) when *M* after nonlinear PAWS was reduced to about 2-3, counting the "residual" darker speckle grains in **FIG. 10b.** The 1D profiles across the focus (green solid curves) measure 5.1 and 7.1 μιτι along *x* and y, respectively. The dashed circles show the measured transducer focal region (50 MHz, - 6 dB). Its lateral profiles (blue dashed curves) measure a FWHM of 65 μιτι. The intensity values in **FIG. 10a** and **FIG. 10b** are normalized to the mean intensity of the image in **FIG. 10a.**

[0088] In speeding up the iterative digital wavefront shaping from current LCoS SLM switching speed of about 60 Hz (although it needs about 1.2 s for a stable image) to ferromagnetic SLM switching speed of about 1 kHz results in an improvement factor of about 16X. Changing to MEMS-DMD switching speed of at least 20 kHz leads to an improvement factor of about 320X.

[0089] A nonlinear PAWS approach may be used to break the ultrasonic resolution limit and achieve both optical resolution focusing inside scattering media and a high peak-enhancement factor. While whole blood may be used as the absorbing target in one aspect, the Grueneisen relaxation effect exists broadly in many materials. Therefore, similar performance may be acquired with other types of absorbers. Furthermore, the system may be engineered to respond much faster. Nonlinear PAWS opens an avenue for many micrometer-scale optical applications, including imaging, therapy, and manipulation, inside highly scattering media.

[0090] The system setup is schematically illustrated in **FIG. 7a,** with more details shown in **FIG. 11.** The system in **FIG. 11** may include a blood layer **710;** a ground glass diffuser **708;** a digital delay generator (DDG) **724;** a half-wave plate (HWP) **706;** lenses **726, 728, 730, and 732;** a neutral density filter (NDF) **734;** a neutral density filter wheel (NDFW) **736;** a microscopic objective (10*, 0.25 NA) **738;** an oscilloscope **718;** signal amplifiers **716;** a polarizing beam splitter (PBS) **702;** a computer **720;** a photodiode **740;** a spatial light modulator (SLM) **704;** a triggering signal **742;** and an ultrasonic transducer (UT) **714.** The system may further include a laser **744** and a circulator **746.** In an aspect, a 532 nm pulsed laser may be used. The laser may produce about 10 ns pulses (pulse energy ≤ about 0.2 mJ) at an adjustable pulse repetition rate of about 0-30 kHz. The laser beam may be directed through a half-wave plate and a polarizing beam splitter to sample a small fraction of the beam. Light reflected by the beam splitter may be attenuated and measured using a photodiode and may be used to compensate for energy fluctuations of the laser output. Light transmitted by the beam splitter may be expanded, and then reflected off a liquid-crystal-on-silicon based phase-only SLM. The SLM may have an aperture of about 16 mm by about 9 mm, with a resolution of about 1920x1 080 pixels. The SLM may be evenly divided into about 192 χ 108 blocks, each independently controlled, with a linearized phase shift between about 0 and about $2\pi$. The reflected beam may be condensed using a set of lenses, and focused by a microscopic objective onto a ground glass diffuser. In an aspect, the objective may be 10X, NA=0.25. A neutral density filter wheel between the SLM and the objective lens may reduce the laser fluence in nonlinear PAWS to avoid thermal saturation . A circular container of bovine blood was placed 10 mm away from the diffuser to serve as the absorptive target for PA sensing. The circular container may be about 15 mm diameter and about 4 mm height. A focused ultrasonic transducer (homemade based on a non-focusing transducer; more details below) may be positioned on the other side of the blood layer to detect the PA signal. Both the

blood layer and ultrasonic transducer may be immersed in water for acoustic coupling. The water may be maintained at room temperature by circulation.

[0091] The PA signals generated may be amplified by about 50 dB, digitized by an oscilloscope at a bandwidth larger than about 500 MHz, and sent to a computer. The linear and nonlinear PA amplitudes may be quantified in MATLAB, and a genetic algorithm may control the optimization. The phase map may be displayed on the SLM using a graphics card. A digital delay generator may control the synchronization between the laser and the oscilloscope. For linear PAWS, one pulse may be fired about every 20 ms. For nonlinear PAWS, two pulses may be fired with a delay of about 40 μs, but the burst period may remain at about 20 ms. After the optimization, the blood layer may be moved off the optical path, and a CCD camera may be attached to a microscope—with a resolution of about 1 μηη/pixel—may be used to image the optical field at the ultrasound focal plane **(FIG. 10a** and **FIG. 10b),** when the initial and final phase patterns are displayed on the SLM, respectively.

## EXAMPLES

### Example 1: The Grueneisen-relaxation effect

[0092] The Grueneisen-relaxation effect was experimentally validated by imaging red blood cells (RBCs). A monolayer of RBCs was fixed on a glass slide, immersed into deionized water, and positioned in the optical focal plane. Multiple PA images were acquired using two-dimensional raster scanning. At each measurement, the PA amplitude was calculated from the average signal of the entire PA image.

[0093] First, the linear relationship was validated between the single-pulse PA amplitude and the excitation laser pulse energy. To avoid the Grueneisen-relaxation effect, only one laser was triggered at 10 kHz. Laser energy was set from 0 to 60 nJ. **FIG. 2a** shows that the single-pulse PA amplitude was proportional to the laser pulse energy.

[0094] Then the Grueneisen-relaxation effect was experimentally demonstrated using two lasers that were sequentially triggered with a 500 ns delay. $\Delta PA_2 = PA_2 - PA_{2\_0} - PA_2$ was the second PA amplitude, whereas $PA_{2\_0}$ was the second PA amplitude measured after the first laser was turned off. Both laser pulse energies were chosen within the linear PA range. The first laser pulse energy was tuned from 0 to 25 nJ while the second laser pulse energy was held at 25 nJ. The second laser PA amplitude ($PA_2$) increased from its baseline (**$PA_{2\_o}$**) while the first laser pulse energy was increased from 0 to 25 nJ. **FIG. 2b** shows a linear relationship between the percentage increase of the second laser PA amplitude and the first laser pulse energy. The largest increase of the second PA amplitude was 14%. According to the linear relationship between water's Grueneisen parameter and temperature, the highest residual temperature rise was estimated to be 3 °C.

[0095] The dependence of the Grueneisen-relaxation effect on the time delay between the two pulses was also quantified. Both of the laser pulse energies were set to 25 nJ. The time delay was tuned from 75 ns to 5 μs. As shown in **FIG.2c,** the amplitude increase of the second PA signal follows an exponential function of the time delay with a decay constant of 0.63 μs, which validates that the coefficient $b$ in Eq. 11 relates to the time delay between the two pulses. For thermal diffusion in water, the characteristic dimension of the heated region was approximately $\sqrt{4\alpha\tau} = 0.57$ μιτι, where $\alpha$ is water's thermal diffusivity of $1.3 \times 10^{-3}$ $cm^2/s$, and $\tau$ is the residual temperature decay time of 0.63 μs. This dimension matches the measured OR-PAM lateral resolution of 0.65 μιτι (see below). Hence, the Grueneisen-relaxation effect was well maintained within the sub-microsecond scale.

**Example 2: Measurement of lateral and axial resolutions**

[0096] Lateral resolution was measured by imaging a sharp ink edge on a cover glass. The edge spread function (ESF) of the GR-PAM was obtained by scanning across the sharp edge **(FIG. 3a).** For comparison, the ESF of the OR-

PAM was computed from the PA signal of the first laser pulses. Derivation of the ESFs gives the line spread functions (LSFs, inset in **FIG. 3a).** The FWHM of the LSF quantifies the lateral resolution. The lateral resolutions of OR-PAM and GR-PAM were 0.65 μιτι and 0.41 μιτι, respectively. Therefore, the lateral resolution was improved by a factor of 1.6, close to the theoretical prediction of V2. In an aspect, the FWHM of the OR-PAM profile may be 45 μιτι.

[0097] Axial resolution was quantified by scanning perpendicularly to a monolayer of RBCs. At each axial position, the peak-to-peak amplitude of the differential PA signal was recorded to form a 1D depth-resolved image of the GR-PAM, which was fitted to a Gaussian function. The FWHM of the Gaussian curve is 2.3 μιτι, which is close to the theoretical prediction of 2.4 μιτι. For comparison, the A-line of the OR-PAM was obtained by converting a time-resolved PA signal into a depth-resolved signal with the known sound speed in water. The envelope of the OR-PAM A-line was calculated using the Hilbert transformation. The FWHM of the envelope is 45 μιτι. Clearly, GR-PAM provides an optical axial resolution much higher than the acoustic axial resolution.

**Example 3: Optical sectioning imaging of red blood cells**

[0098] GR-PAM enables optical sectioning, improving the axial resolution. **FIG. 4a, FIG. 4b,** and **FIG. 4c** show GR-PAM images of a monolayer of RBCs placed at different axial positions. The average laser pulse energy was set at 25 nJ. As the RBCs moved out of optical focus, the GR-PA signals quickly decreased, demonstrating optical sectioning. **FIG. 4d, FIG. 4e,** and **FIG. 4f** present OR-PAM images of the same sample. The OR-PAM signals did not show obvious changes when scanning the sample along the axial direction. **FIG. 4g** and **FIG. 4h** present GR-PAM and OR-PAM side-view images in the *x-z* plane. With optical axial resolution, a small tilt angle of the sample slide was clearly imaged using GR-PAM. In addition to the improvement in the axial resolution, GR-PAM also enhanced image contrast. The doughnut-feature contrast was quantified as $c = (p_{A_{max}} - p_{A_{min}}) / p_{A_{max}}$, where $p_{A_{min}}$ is the smallest pixel

value in the doughnut feature, and $PA_{\max}$ is the nearest peak value around the doughnut center, as shown in **FIG. 4i.** GR-PAM shows clearer features of the doughnut-shaped red blood cells than OR-PAM. The contrasts of the doughnut-shaped features were measured in GR-PAM and OR-PAM images. Based on measurements from 9 RBCs, the contrast of GR-PAM is 0.46±0.04; and the contrast of OR-PAM is 0.1 1±0.03 (mean ± standard error). The average ratio between the contrasts is 4.2. GR-PAM increased the average contrast by a factor of 4.2.

**Example 4: Calibration-free measurement of absolute absorption coefficient**

[0099] The optical absorption coefficient is directly related to the molecular molar extinction coefficient and concentration. By measuring the optical absorption coefficient, the concentration of molecules may be readily determined with a known molar extinction spectrum. One example is to measure the oxy- and deoxy-hemoglobin concentrations in blood, which are important functional parameters associated with tissue oxygenation. PA amplitude is proportional to the optical absorption coefficient and local optical fluence, which makes PA imaging an ideal tool to probe the absorbers' concentration. In order to determine the absolute absorption coefficient from conventional PA signals, the local optical fluence was calibrated. However, the calibration may be challenging in an inhomogeneous medium. For example, other scatterers or absorbers on the optical path might shadow the region of interest, leading to inaccurate fluence calibration. Owing to its optical sectioning capability and absorption contrast, GR-PAM enables a unique approach to the quantification of the absolute absorption coefficient without fluence calibration.

[00100] According to Beer's law, the transmitted optical energy decays exponentially with the optical path length. In an absorption-dominant sample, i.e., optical absorption is much stronger than scattering, the optical energy $E$ can be expressed as a function of penetration depth $z$ as follows:

$$E(z) = E_0 \exp(-\mu_a z), \quad (13)$$

where $E_Q$ is the pulse energy on the absorber surface. According to Eq. 7, the GR-PA signal is proportional to the square of the optical energy. When scanning the GR-PAM focus along the z-axis, the GR-PA signal becomes a function of penetration depth z:

$$Ay(z) = kb\eta_{th}^2 E_0^2 \exp[-2\mu_a(x, y, z)z] \iint \mu_\alpha^2(x, y, z) \frac{1}{\pi^2 w^4} \exp(-2\frac{x^2 + y^2}{w^2})dxdy . \quad (14)$$

[00101] If the absorption coefficient is assumed to be uniformly distributed, then Eq.14 can be re-written as

$$Ay(\zeta) = kb\eta_{th}^2 \mu X \frac{1}{2\pi w^2} \exp(-2\mu_a z) . \quad (15)$$

Eq. 15 shows that the GR-PA signal is an exponential function of penetration depth. The decay constant is twice the absolute absorption coefficient. Although the laser pulse energy at the absorber surface may change due to shadowing from other objects, the exponential decay constant of the GR-PA signal will not be affected. Therefore, the absorption coefficient can be determined without fluence calibration.

[00102] GR-PAM was demonstrated to be able to probe the interior of a relatively large absorber. **FIG. 5a** shows a diagram of a semi-infinite blood sample. The sample was imaged by both OR-PAM and GR-PAM in the *x-z* plane, with an average laser pulse energy of 15 nJ. The two-dimensional The OR-PAM image in **FIG. 5b** shows good contrasts only on the upper boundary of the blood sample due to the "boundary buildup", referred to as specular emission here. Although a significant number of photons can penetrate beyond the boundary, the OR-PAM signal shows no obvious contrast beyond the boundary. **FIG. 5c** is a two-dimensional GR-PAM image, which shows clear signals from deep blood. **FIG. 5d** shows two depth-resolved PA signals from a pair of laser pulses and their difference. The optical focus was placed 60 μιτι below the

boundary. The two raw PA signals were almost identical at the boundary, but were very different at the focus. Thus in the GR-PA signal, the specular emission was suppressed, but the signal from the optical focal zone was effectively recovered because of the Grueneisen-relaxation effect.

[00103] **FIG. 5e** shows that the GR-PA signal decreases with the penetration depth. The data was fitted to Eq. 15 to recover the absolute absorption coefficient. By diluting the blood sample into different concentrations, different absorption coefficients were measured. The results agree well with the actual absorption coefficients measured with a spectrophotometer. For example, the actual absorption coefficient of 100% blood at 532 nm was measured to be 234 $cm^{-1}$, which validated the GR-PAM measurement of 240±8 $cm^{-1}$.

**Example 5: PAWS**

[00104] The PAWS system setup is illustrated schematically in **FIG. 7a.** The system may include a polarized beam splitter (PBS) **702,** a spatial light modulator (SLM) **704,** a half-wave plate (λ/2) **706.** The scattering medium consists of a ground glass diffuser **708** and a layer of optically absorbing whole blood **710.** The incident light reflected from the SLM surface was scattered by a diffuser **708,** generating a random speckle pattern with about 5-μιτι speckle grains on the blood layer **710.** The system further included a lens **712,** an ultrasonic transducer **714,** an amplifier **716,** an oscilloscope **718,** and a computer **720** with a genetic algorithm **722.** The whole blood **710** and the ultrasound transducer **714** may be within water **748.** A photodiode measured laser energy fluctuations to compensate for the PA signals. The pulse energy on the blood layer was about 0.1 mJ, within an illuminated area of about 1 $cm^2$, which corresponded to a fluence of about 0.1 $mJ\text{-}cm^{-2}$. Initially, no nonlinear PA signals were observable even at the full energy output of the laser. In order to generate detectable nonlinear PA signals, the optical fluence needs to be sufficiently high (>5 $mJ\text{-}cm^{-2}$ for whole blood). Therefore, to increase the optical fluence within the PA sensing region, linear PAWS (Stage 1) was first conducted before nonlinear PAWS

(Stage 2). For both stages, the SLM was divided into 192x1 08 independently controlled blocks, and a genetic algorithm was used to optimize the phase pattern on the SLM.

[00105] FIG. **8a** and FIG. **8b** shows experimental results of Stage 1—using linear PA signal as feedback for wavefront shaping (linear PAWS) optimization. In linear PAWS (Stage 1), single laser pulses were fired every 20 ms to generate the PA signals. An initial PA signal (inset of FIG. **8a),** averaged over 16 traces, was recorded by displaying a random phase pattern on the SLM. Note that all PA signals were compensated for laser energy changes, and normalized to the initial PA peak-to-peak amplitude shown here. As shown in FIG. **8b,** the PA amplitude increased as the linear PAWS optimization proceeded, corresponding to increased optical energy within the acoustic focus. Linear PA amplitude improved -60 times in Stage 1, indicating a peak enhancement factor of -60 for optical fluence within the acoustic focus. The algorithm was terminated after 800 iterations, when the PA amplitude increased -60 times over the initial signal (FIG. **8a).** The fluence within the acoustic focus was estimated to increase from about 0.1 to about 6 mJ-cm$^{-2}$. Further enhancement was not seen with linear PAWS, as indicated by the relatively flat response after the 600$^{th}$ iteration.

[00106] FIG. **9a,** FIG. **9b,** and FIG. **9c** summarize experimental results of Stage 2—using nonlinear PA signal as feedback for wavefront shaping (nonlinear PAWS) optimization. The final phase map from Stage 1 was used as the starting point for nonlinear PAWS (Stage 2). In the nonlinear PAWS experiment, a pair of pulses were fired, separated by 40 μs (limited by the maximum laser repetition rate), well within the thermal confinement time of 189 μs (estimated based on a speckle size of about 5 μιτι and a thermal diffusivity of about 1.3x1 0$^{-3}$ cm$^2$-s$^{-1}$). The initial PA signals, obtained by using the phase map from Stage 1, are shown in FIG. **9a.** The difference between the two PA signal amplitudes $\Delta V$ was used as feedback in nonlinear PAWS. The final PA signals after 1600 iterations are shown in FIG. **9b,** which also shows the optimized phase pattern displayed on the SLM as an inset. Note that the shown signals have been compensated for

the laser pulse energy adjustments shown in **FIG. 9c.** The first PA signal remained relatively constant before and after nonlinear PAWS, but the second PA signal was dramatically enhanced because of the Grueneisen relaxation effect. The inset shows the final optimized phase pattern displayed on the SLM. The increase of the nonlinear PA amplitude with iteration in Stage 2 is shown in **FIG. 9c.** As seen, the final nonlinear PA amplitude was ~100 times greater than the initial value, indicating a ~100-time improvement of the peak fluence. To avoid overheating the blood during the optimization, the laser energy was attenuated by 10% every 300 iterations. This attenuation caused the measured $\Delta V$ to change between each of the six adjustments in the experiment. The algorithm therefore re-measured $\Delta V$ at the start of each stage. All other parameters were kept constant between consecutive stages. The change in energy was compensated for in the results shown in **FIG. 9b** and **9c.** The nonlinear signal increased in every stage but the last, indicating that by the end of the nonlinear optimization, the focal spot had approached its smallest size. Nonlinear PA amplitude improved ~100 times during Stage 2. 1600 iterations were used, with the incident laser energy ***(E)*** attenuated by 10% every 300 iterations to avoid overheating the sample. The normalized laser energy $R = E/E_{max}$ is also shown, where $E_{max}$ was the initial laser energy used before adjustment. The compensated nonlinear PA amplitudes are given by $\Delta V / R^2$, and the nonlinear improvement factor is therefore given by $\frac{\Delta V / R^2}{\Delta V_{initial}}$.

[00107] The optical field was imaged at the ultrasound focal plane using a CCD. When a random phase pattern was displayed on the SLM, a speckle pattern **(FIG. 9a)** was captured with randomly distributed speckle grains. The FWHM of the acoustic focus is shown by the dashed circle. Note that there are many speckle grains within the acoustic focus. When the optimized phase pattern from nonlinear PAWS was displayed, a focal spot with the size of a single

speckle grain was formed **(FIG. 9b).** The size of the focal spot was measured to be 5.1 μm × 7.1 μιτι (FWHM), which is ~10 times smaller than that of the acoustic focus.

**Example 6: Transducer field calibration.**

[00108] A 50-MHz focused ultrasonic transducer was used in the experiment. The transducer was modified in-house from a non-focusing transducer (V358, Panametrics NDT, USA) by adding an acoustic focusing lens. Due to the high center frequency, the typical method of characterizing the transducer using a hydrophone or a pulser-receiver cannot be used. Instead, acoustic phase conjugation was used from a metal ball (8 mm diameter) to measure the acoustic focal zone. The transducer axial focus was measured to be 11.425 mm from the transducer, and the lateral FWHM of the focal region was 65 μιτι. **FIG. 12a** and **FIG. 12b** summarize the focus calibration of the 50 MHz transducer. In **FIG. 12a,** a function generator **750** (FG; DG41 62, Rigol) generates a burst including 10 cycles of 50 MHz sine waves, with a peak-to-peak amplitude of 5 V. The burst is sent to the ultrasonic transducer (UT) **714,** which emits an acoustic burst correspondingly. The acoustic wave is reflected by the metal ball, and received by the transducer. The echoed signal is digitized using an oscilloscope **718** (Osc; TDS 5034, Tektronix). The peak-to-peak value is proportional to the acoustic pressure amplitude at each position. In experiment, the transducer is moved along the z direction first to determine the axial focal plane, and then scanned along the y direction to characterize the lateral profile at the focal plane. In **FIG. 12b,** the squares are measured data, and the curve is a Gaussian fit. The acoustic focal profiles shown in **FIG. 10b** are based on the interpolation of the measured data.

**Example 7: Speckle size.**

[00109] By calculating the autocorrelation of the speckle pattern imaged before wavefront-shaping optimization, the speckle grain size was measured at

the ultrasound focal plane to be about5 μηη. This measurement was consistent with both the final experimental optical focus size, and the estimated value using the equation $\lambda \times L / D$, where λ = 0.532 μιτι is the optical wavelength, $L$ = 10 mm is the distance from the diffuser to the absorber, and $D$ « 1 mm is the size of the beam illuminating the diffuser.

## CLAIMS

What is claimed is:

1. A method of focusing a light pulse within a focus area using nonlinear photoacoustic wavefront shaping (PAWS), the method comprising:

obtaining an initial Grueneisen-relaxation photoacoustic (GR-PA) feedback signal using an initial wavefront from within the focus area;

obtaining at least one subsequent GR-PA feedback signal, each subsequent GR-PA feedback signal obtained using a subsequent wavefront determined by altering a preceding wavefront according to a wavefront optimization rule using an immediately preceding GR-PA feedback signal obtained using the preceding wavefront;

selecting an optimized wavefront according to an optimization criterion; and

focusing the light pulse comprising the optimized wavefront within the focus area at a single-speckle resolution.

2. The method of claim 1, wherein a GR-PA signal is obtained by:

delivering a first laser pulse comprising one wavefront to the focus area;

detecting a first photoacoustic signal induced by illumination of the focus area by the first laser pulse;

delivering a second laser pulse comprising the one wavefront to the focus area at a lag interval time after the delivery of the first laser pulse;

detecting a second photoacoustic signal induced by illumination of the focus area by the second laser pulse; and

subtracting a first peak-to-peak amplitude of the first photoacoustic signal from a second peak-to-peak amplitude of the second photoacoustic signal to obtain the GR-PA signal.

3. The method of any one of the preceding claims, wherein each subsequent wavefront produces a subsequent GR-PA signal higher than any preceding GR-PA signal.

4. The method of any one of the preceding claims, wherein the wavefront optimization rule comprises a genetic algorithm.

5. The method of any one of the preceding claims, wherein the optimization criterion is chosen from:

the optimized wavefront is the wavefront determined after a maximum number of GR-PA signals have been obtained;

the optimized wavefront is the wavefront for which a difference a GR-PA signal associated with the optimized wavefront and the immediately preceding GR-PA signal is less than a minimum GR-PA signal difference; and

the optimized wavefront produces a GR-PA signal greater than a minimum threshold GR-PA signal.

6. The method of any one of the preceding claims, wherein the maximum number of GR-PA signals ranges from about 100 to about 2000.

7. The method of any one of the preceding claims, wherein the lag interval time is less than about 50 μs.

8. The method of any one of the preceding claims, wherein each wavefront comprises a spatial phase pattern generated by delivering a laser pulse through a configurable spatial light modulator.

9. The method of any one of the preceding claims, wherein the initial wavefront is chosen from a random spatial phase pattern and an optimal spatial phase pattern obtained by a linear photoacoustic wavefront shaping method.

10. The method of any one of the preceding claims, wherein the focus region of the GR-PA signal comprises a lateral resolution of less than about 10 μιτι.

11. The method of any one of the preceding claims, further comprising centering the focus region within the acoustic focus region by:

obtaining a plurality of scanned PA signals using the optimized wavefront scanned across the acoustic focus region at a plurality of scan locations, wherein the optimized wavefront is scanned across the acoustic focus region by applying a linear phase ramp to an optimized spatial phase pattern associated with the optimized wavefront; and

using the scan location associated with the highest PA signal of the plurality of scanned PA signals to center the focus region within the acoustic focus region.

12. The method of any preceding claim, wherein a high-fluence laser pulse comprising the optimized waveform is delivered to the focus region to perform a laser microsurgery, the laser microsurgery comprising a photocoagulation of small blood vessels, a photoablation of tissue, and any combination thereof.

13. A method of Grueneisen-relaxation photoacoustic microscopy (GR-PAM) of a subject, the method comprising:

delivering a first laser pulse to a focus region;

detecting a first photoacoustic signal induced by illumination of the focus region by the first laser pulse;

after a lag interval time after the delivery of the first laser pulse, delivering a second laser pulse to the focus region, wherein the lag interval time is less than a thermal relaxation time of the subject;

detecting a second photoacoustic signal induced by illumination of the focus region by the second laser pulse; and

subtracting a first peak-to-peak magnitude of the first photoacoustic signal from a second peak-to-peak magnitude of the second photoacoustic signal to obtain a GR-PA signal corresponding to the focus region.

14. The method of claim 13, wherein the lag interval time is less than or equal to about 20 *[is.*

15. The method of any one claims 13 - 14, wherein the first laser pulse and the second laser pulse each comprise a pulse width of less than or equal to about 10 ns.

16. The method of any one of claims 13 - 15, wherein the lateral resolution of the GR-PAM is less than about 0.5 μιτι.

17. The method of any one of claims 13 - 16, wherein GR-PAM performs optical sectioning at an axial resolution of less than about 5 μιτι.

18. A method of obtaining an absorption coefficient of a sample using Grueneisen-relaxation photoacoustic microscopy (GR-PAM), the method comprising:

obtaining a plurality of GR-PA signals , each GR-PA signal obtained at a focus region situated at a different penetration depth *z* within the sample;

fitting the plurality of GR-PA signals and associated penetration depths *z* to a first equation to determine an optical absorption coefficient $\mu_\alpha$*:*

$$\Delta PA(z) = Ae^{-(2\mu_a z)}$$

wherein ΔPA (ζ) is the GR-PA signal at the penetration depth z and A is an amplitude corresponding to the GR-PA signal measured at z = 0; and

calculating the optical absorption coefficient $\mu_\alpha$ from the fitted first equation.

19. The method of claim 18, wherein each GR-PA signal at each penetration depth z is obtained by:

delivering a first laser pulse to the focus region at the penetration depth z;

detecting a first photoacoustic signal induced by illumination of the focus region by the first laser pulse;

after a lag interval time after the delivery of the first laser pulse, delivering a second laser pulse to the focus region;

detecting a second photoacoustic signal induced by illumination of the focus region by the second laser pulse; and

subtracting a first peak-to-peak magnitude of the first photoacoustic signal from a second peak-to-peak magnitude of the second photoacoustic signal to obtain each GR-PA signal.

20. The method of any of claims 18 - 19, further comprising determining the concentration of a plurality of molecules with a known molar extinction spectrum in the sample using the obtained absorption coefficient, wherein the plurality of molecules are selected from: oxy-hemoglobin or deoxy-hemoglobin.

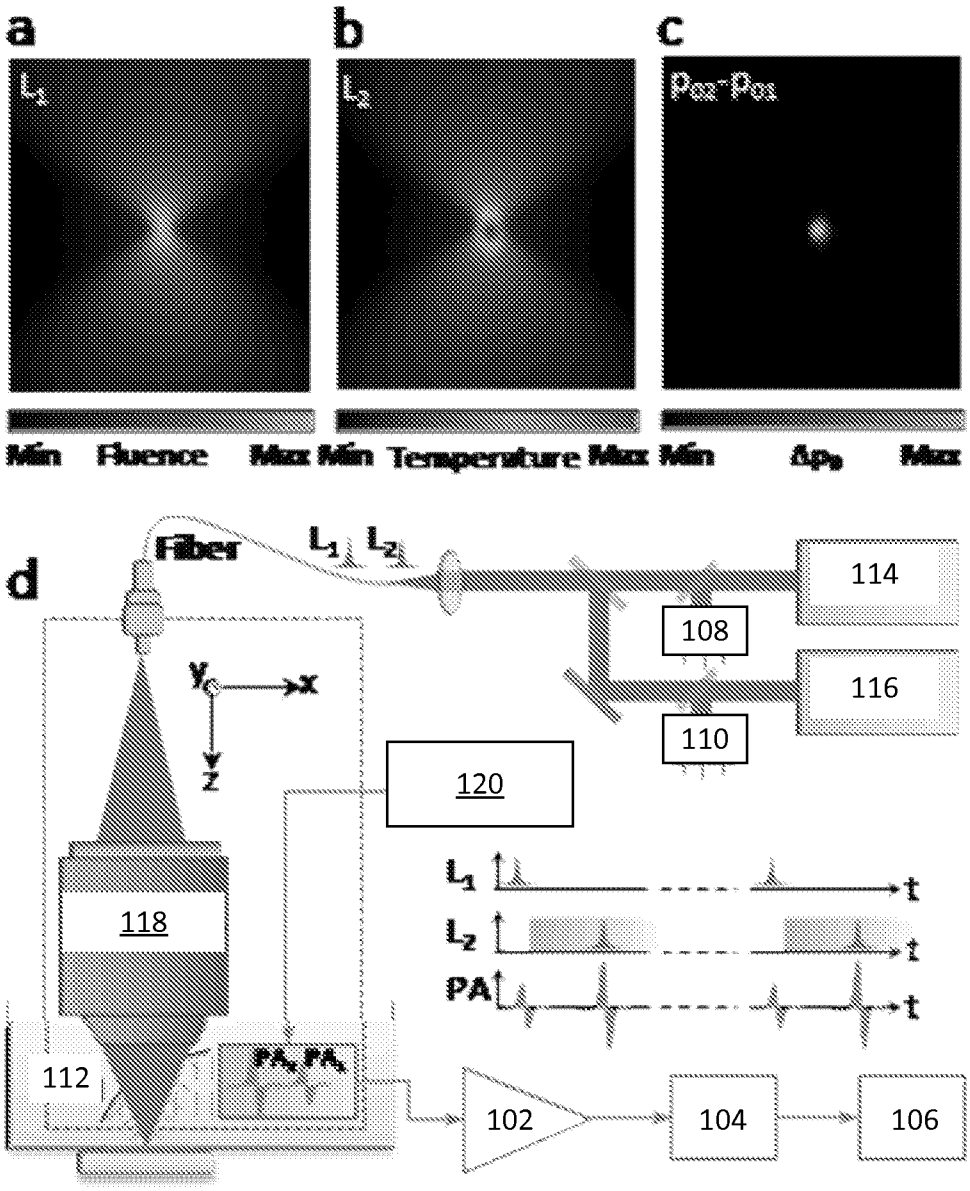
a
b
c
$L_1$
$L_2$
$p_{a2}-p_{a1}$
Min Fluence Max
Min Temperature Max
Min $\Delta p_0$ Max
d
Fiber
$L_1$ $L_2$
114
108
116
110
y
x
z
120
118
$L_1$
$L_2$
PA
t
112
$PA_1$ $PA_2$
102
104
106

FIG. 1

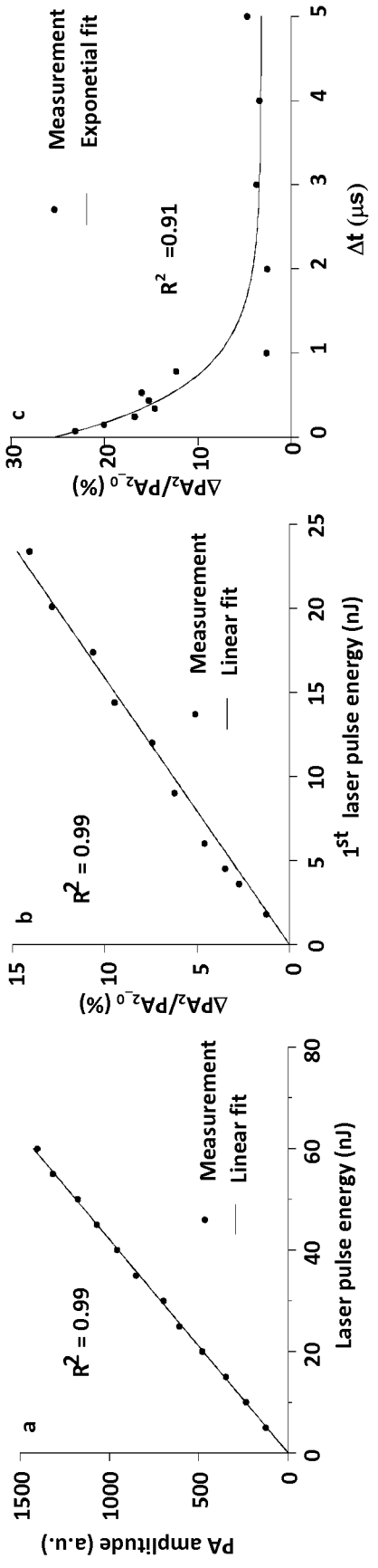
a
PA amplitude (a.u.)
Laser pulse energy (nJ)
R2 = 0.99
Measurement
Linear fit
b
ΔPA2/PA2_0 (%)
1st laser pulse energy (nJ)
R2 = 0.99
Measurement
Linear fit
c
ΔPA2/PA2_0 (%)
Δt (μs)
R2 =0.91
Measurement
Exponetial fit

FIG. 2

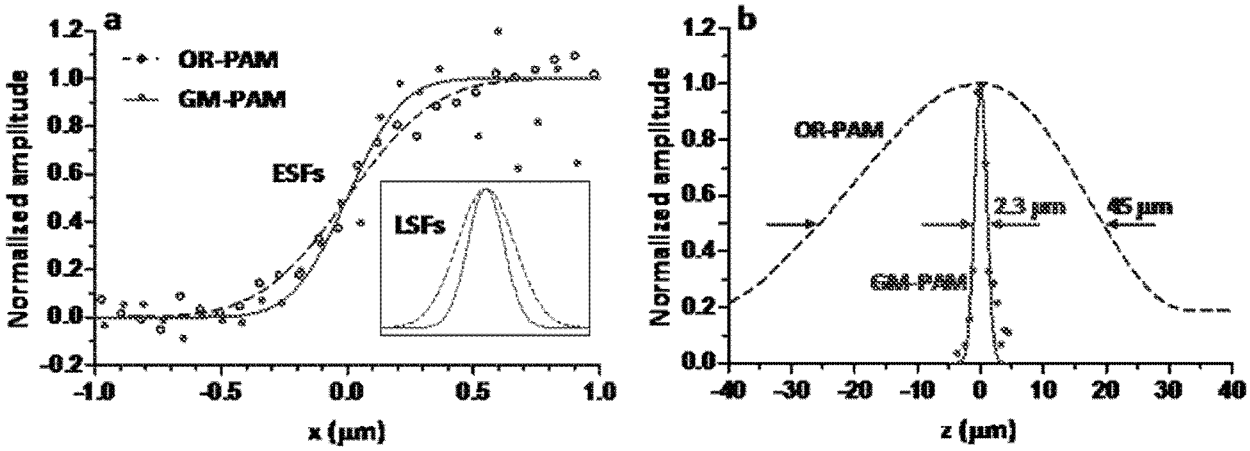
a
OR-PAM
GM-PAM
ESFs
LSFs
Normalized amplitude
x (μm)
b
OR-PAM
GM-PAM
2.3 μm
45 μm
Normalized amplitude
z (μm)

FIG. 3

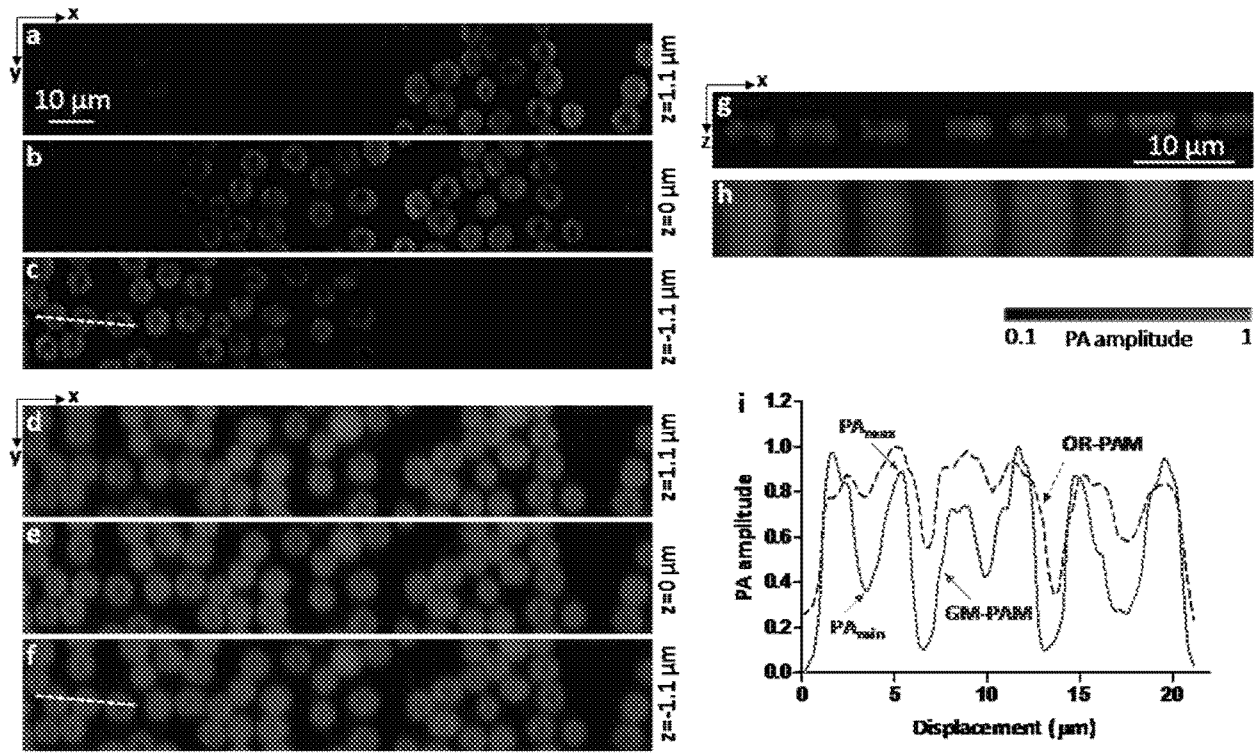
a
10 μm
z=1.1 μm
b
z=0 μm
c
z=-1.1 μm
d
z=1.1 μm
e
z=0 μm
f
z=-1.1 μm
g
10 μm
h
0.1 PA amplitude 1
i
PA amplitude
Displacement (μm)
OR-PAM
GM-PAM

FIG. 4

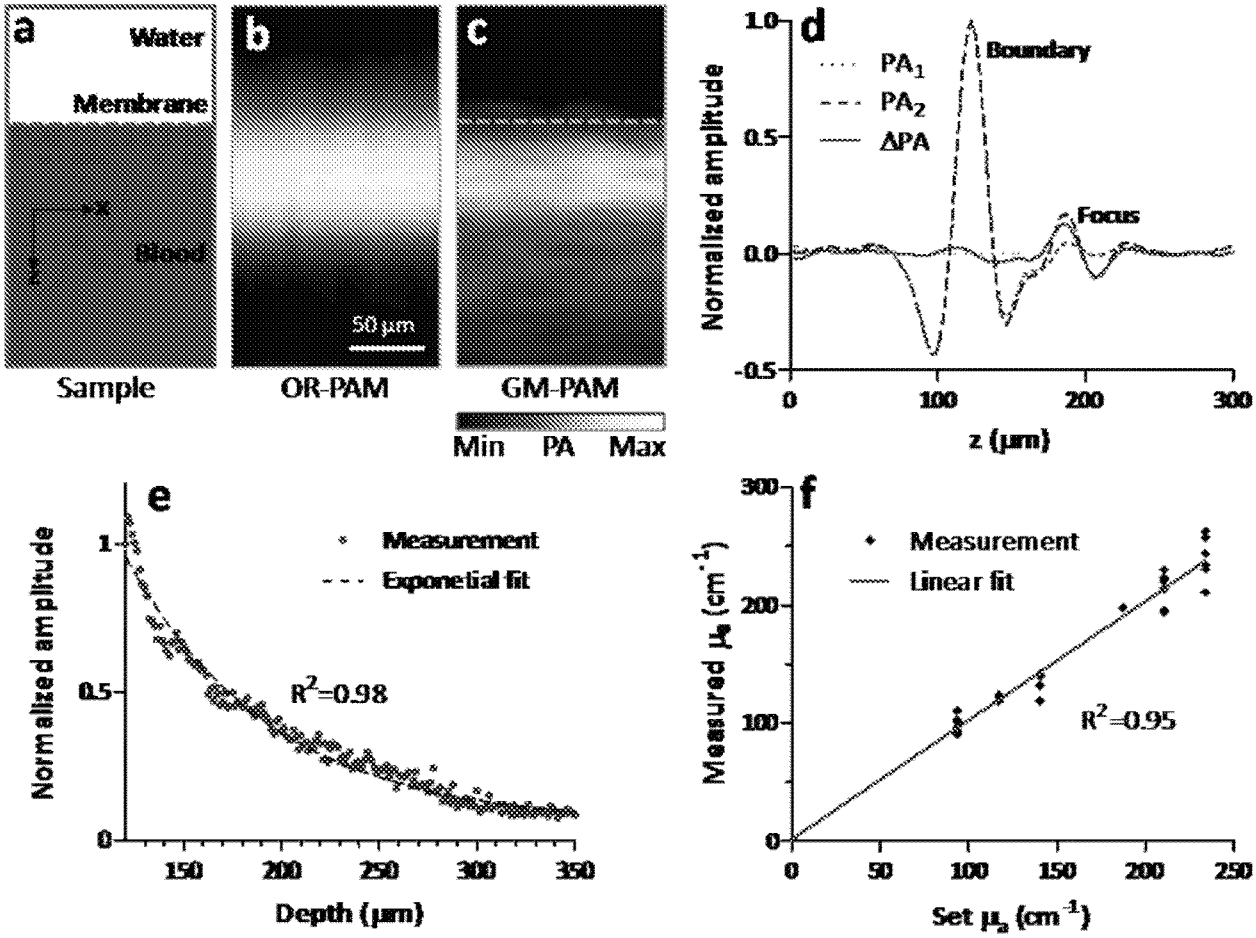
a
Water
Membrane
Blood
z
x
b
50 μm
c
Sample
OR-PAM
GM-PAM
Min PA Max
d
PA1
PA2
ΔPA
Boundary
Focus
Normalized amplitude
z (μm)
e
Measurement
Exponetial fit
R2=0.98
Normalized amplitude
Depth (μm)
f
Measurement
Linear fit
R2=0.95
Measured μs (cm-1)
Set μs (cm-1)

FIG. 5

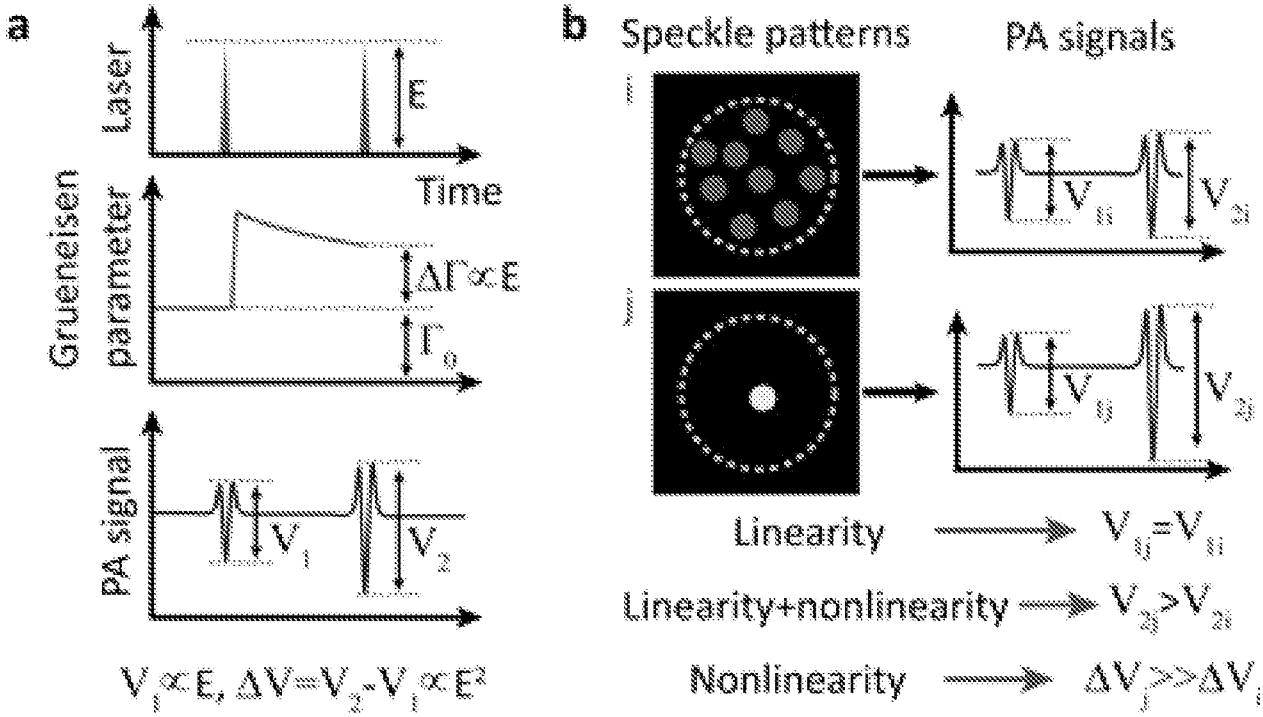
a
Laser
E
Time
Grueneisen parameter
ΔΓ∝E
Γ0
PA signal
V1
V2
V1∝E, ΔV=V2-V1∝E2
b
Speckle patterns
PA signals
i
j
Vi1
Vi2
Vj1
Vj2
Linearity
Vj1=Vi1
Linearity+nonlinearity
Vj2>Vi2
Nonlinearity
ΔVj>>ΔVi

FIG. 6

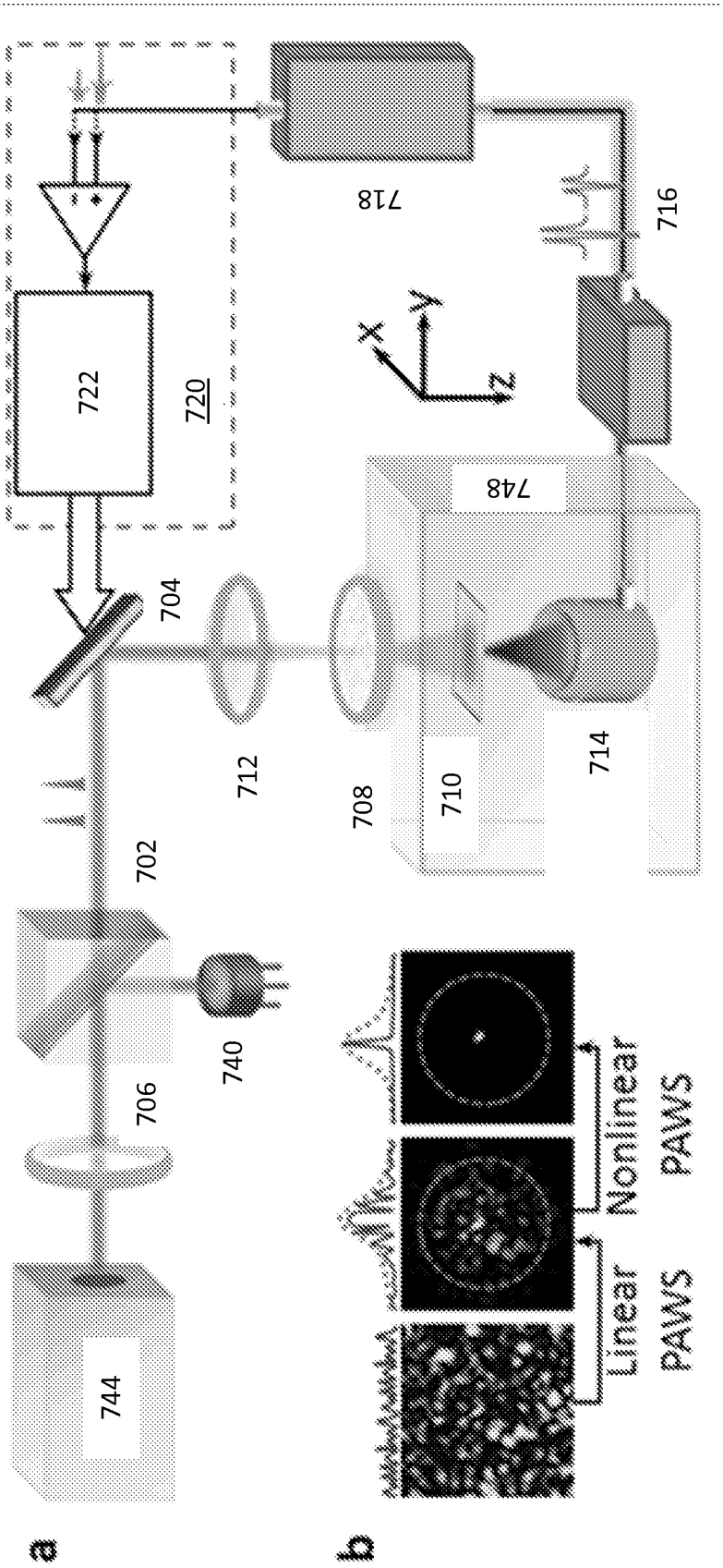
a
b
744
706
740
702
712
708
710
714
704
748
718
716
722
720
x
y
z
Linear PAWS
Nonlinear PAWS

FIG. 7

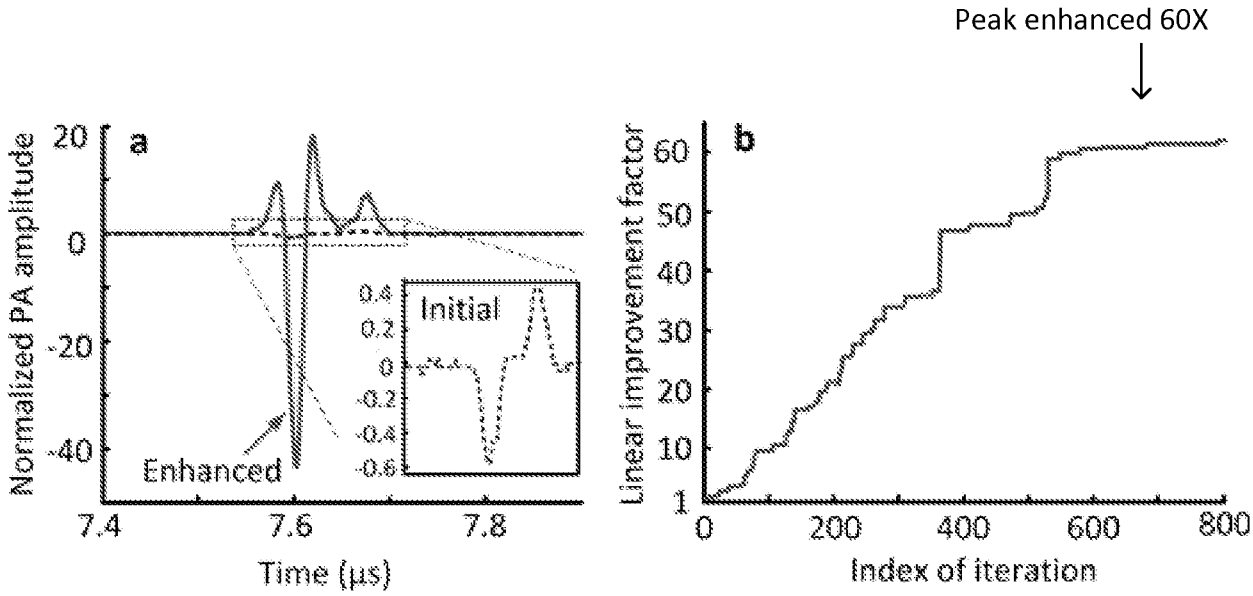
Peak enhanced 60X
a
b
Normalized PA amplitude
20
0
-20
-40
Enhanced
Initial
0.4
0.2
0
-0.2
-0.4
-0.6
7.4
7.6
7.8
Time (μs)
Linear improvement factor
60
50
40
30
20
10
1
0
200
400
600
800
Index of iteration

**FIG. 8**

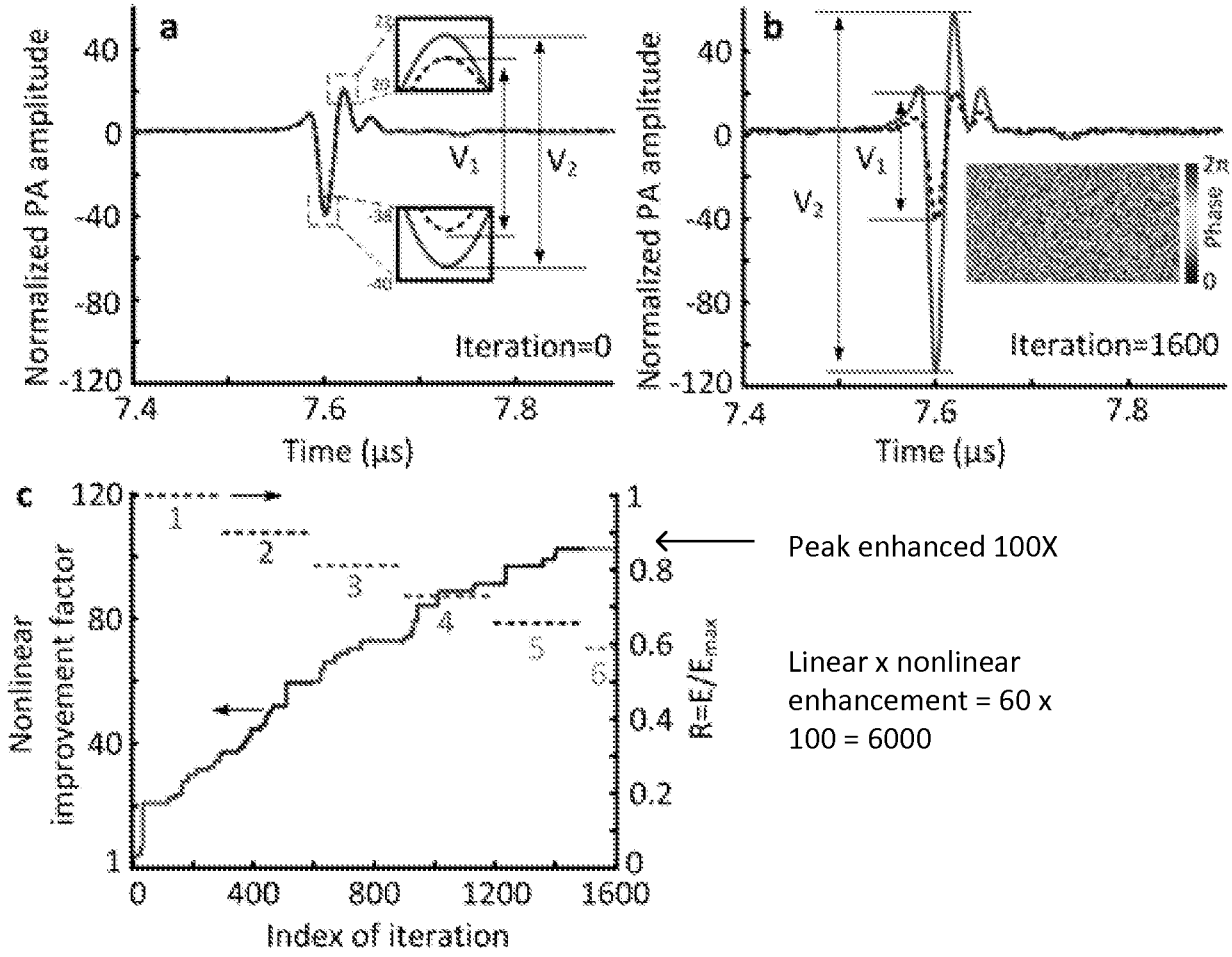
a
b
c
Normalized PA amplitude
Time (μs)
Iteration=0
Iteration=1600
V1
V2
Phase
Nonlinear improvement factor
Index of iteration
R=E/Emax
Peak enhanced 100X
Linear x nonlinear enhancement = 60 x 100 = 6000

FIG. 9

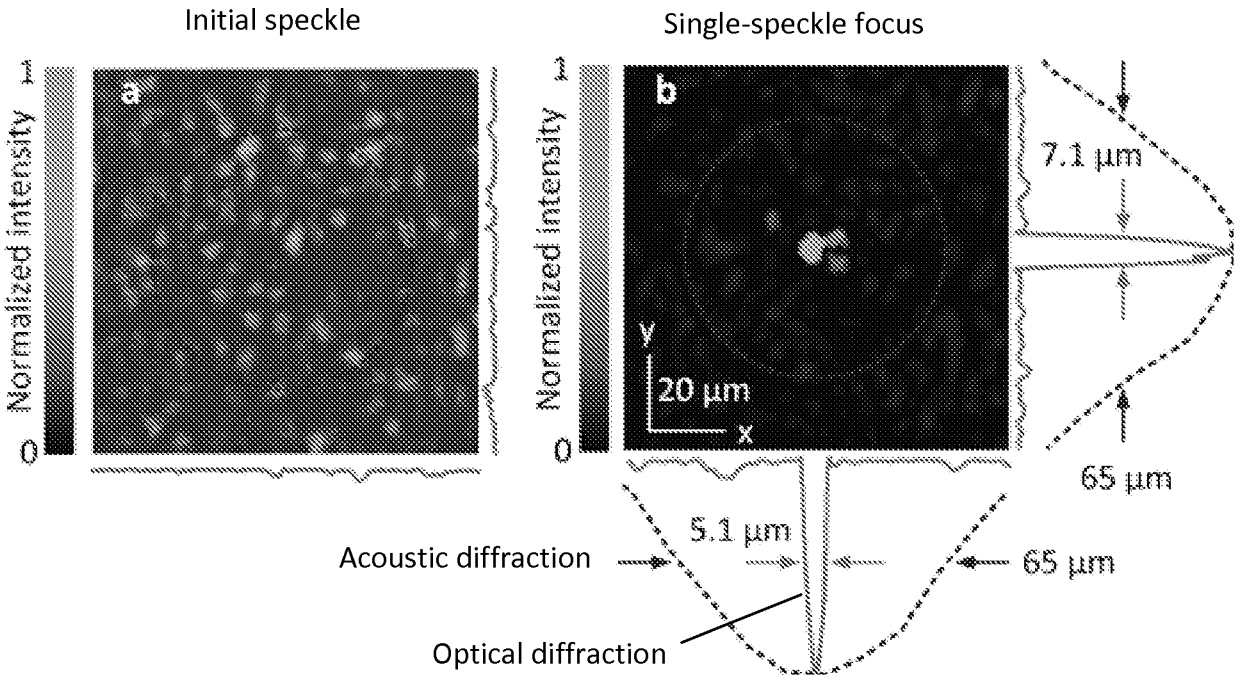
Initial speckle
Single-speckle focus
Normalized intensity
1
0
a
b
y
x
20 µm
7.1 µm
65 µm
5.1 µm
65 µm
Acoustic diffraction
Optical diffraction

FIG. 10

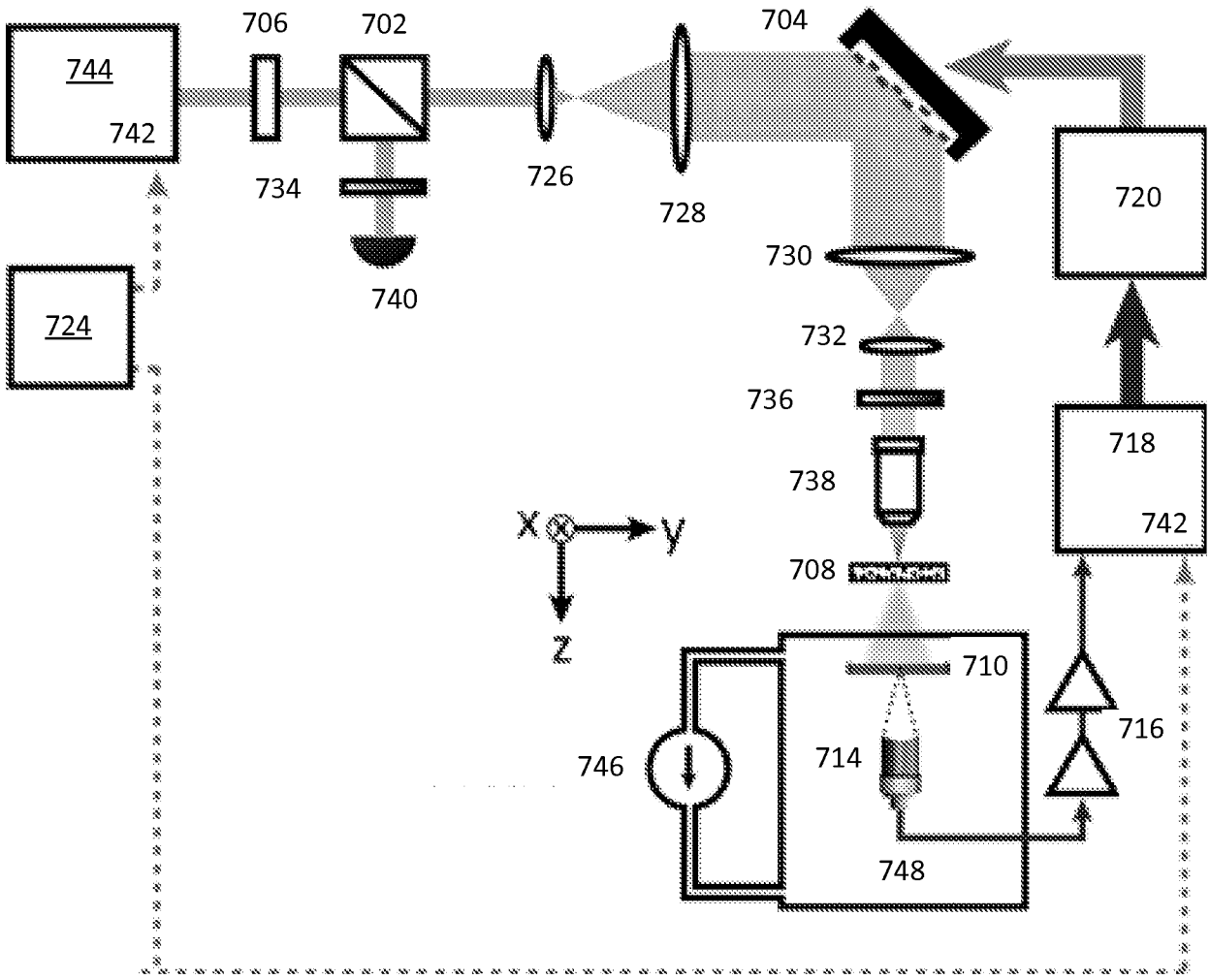
744
742
706
702
704
734
726
728
720
740
730
724
732
736
718
738
742
x
y
z
708
710
716
746
714
748

FIG. 11

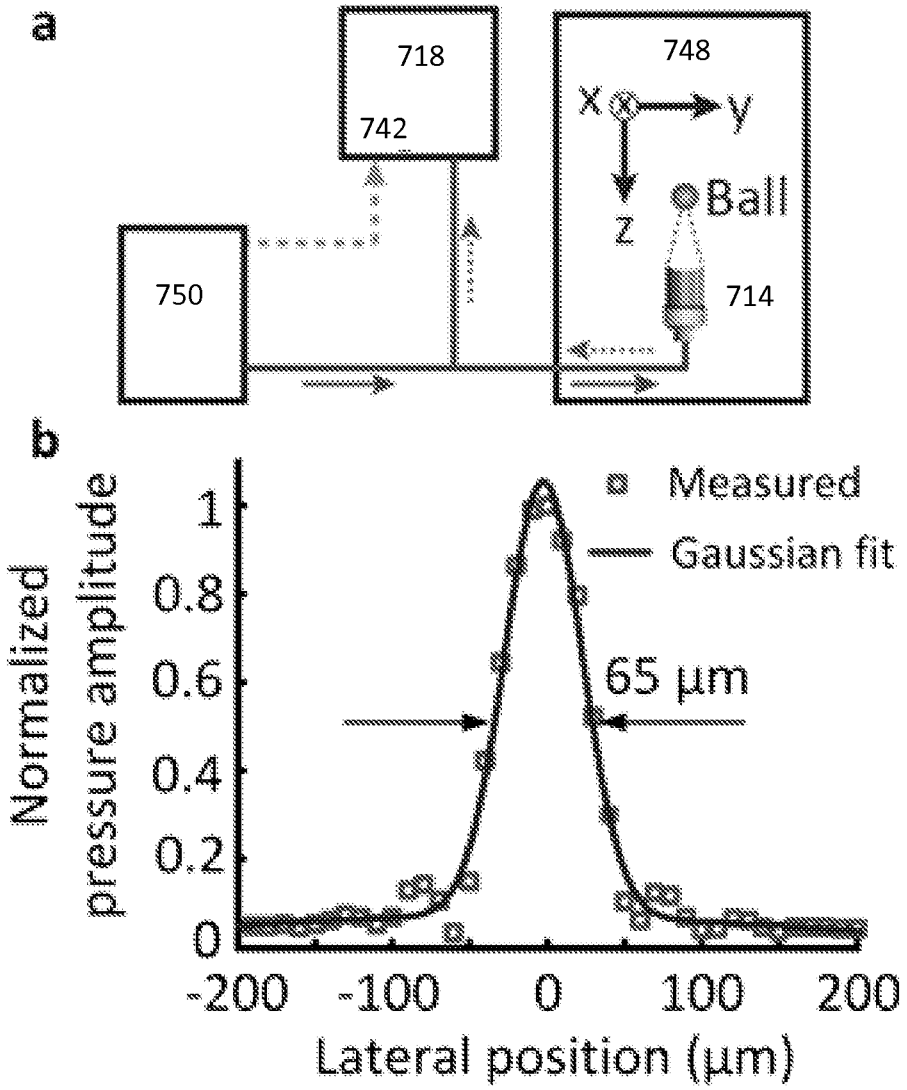
a
718
742
748
x
y
z
Ball
714
750
b
Measured
Gaussian fit
65 µm
Normalized pressure amplitude
1
0.8
0.6
0.4
0.2
0
-200
-100
0
100
200
Lateral position (µm)

FIG. 12

**INTERNATIONAL SEARCH REPORT**

International application No.
**PCT/US20 14/066437**

**Box No. II Observations where certain claims were found unsearchable (Continuation of item 2 of first sheet)**

This international search report has not been established in respect of certain claims under Article 17(2)(a) for the following reasons:

1. ☐ Claims Nos.:
because they relate to subject matter not required to be searched by this Authority, namely:

2. ☐ Claims Nos.:
because they relate to parts of the international application that do not comply with the prescribed requirements to such an extent that no meaningful international search can be carried out, specifically:

3. ☒ Claims Nos.: 4-12,16-17
because they are dependent claims and are not drafted in accordance with the second and third sentences of Rule 6.4(a).

**Box No. Ill Observations where unity of invention is lacking (Continuation of item 3 of first sheet)**

This International Searching Authority found multiple inventions in this international application, as follows:

1. ☐ As all required addtional search fees were timely paid by the applicant, this international search report covers all searchable claims.

2. ☐ As all searchable claims could be searched without effort justifying an additional fees, this Authority did not invite payment of any additional fees.

3. ☐ As only some of the required additional search fees were timely paid by the applicant, this international search report covers only those claims for which fees were paid, specifically claims Nos.:

4. ☐ No required additional search fees were timely paid by the applicant. Consequently, this international search report is restricted to the invention first mentioned in the claims; it is covered by claims Nos.:

**Remark on Protest**

☐ The additional search fees were accompanied by the applicant's protest and, where applicable, the payment of a protest fee.

☐ The additional search fees were accompanied by the applicant's protest but the applicable protest fee was not paid within the time limit specified in the invitation.

☐ No protest accompanied the payment of additional search fees.

**INTERNATIONAL SEARCH REPORT**

International application No.
**PCT/US2014/066437**

**A. CLASSIFICATION OF SUBJECT MATTER**

**G02B 21/00(2006.01)i**

According to International Patent Classification (IPC) or to both national classification and IPC

**B. FIELDS SEARCHED**

Minimum documentation searched (classification system followed by classification symbols)
G02B 21/00; A61B 8/00; A61B 5/00; G01N 29/00

Documentation searched other than minimum documentation to the extent that such documents are included in the fields searched
Korean utility models and applications for utility models
Japanese utility models and applications for utility models

Electronic data base consulted during the international search (name of data base and, where practicable, search terms used)
eKOMPASS(KIPO internal) & Keywords: photoacoustic, light pulse, nonlinear, Grueneisen-relaxation, wavefront shaping, feedback signal, optimization criterion, single-speckle resolution, focus area, GR-PA

**C. DOCUMENTS CONSIDERED TO BE RELEVANT**

| Category* | Citation of document, with indication, where appropriate, of the relevant passages | Relevant to claim No. |
|---|---|---|
| X | US 6498942 B1 (ESENALIEV, RINAT O. et al.) 24 December 2002<br>See column 10, line 9 - column 17, line 21 and claims 1,22. | 18,20 |
| A | | 1-3,13-15,19 |
| A | EP 0919180 A1 (TRW INC.) 02 June 1999<br>See abstract; paragraphs [0011]-[0017] ; and claim 1. | 1-3,13-15,18-20 |
| A | US 5977538 A (UNGER, EVAN C. et al.) 02 November 1999<br>See column 1, line 52 - column 2, line 65 and figure 1. | 1-3,13-15,18-20 |
| A | US 5840023 A (ORAEVSKY, ALEXANDER A. et al.) 24 November 1998<br>See abstract; column 1, line 43 - column 2, line 50; and claim 1. | 1-3,13-15,18-20 |
| A | US 5615675 A (CTDONNELL, MATTHEW et al.) 01 April 1997<br>See column 2, line 5 - column 3, line 47 and figure 1. | 1-3,13-15,18-20 |

☐ Further documents are listed in the continuation of Box C.

☒ See patent family annex.

* Special categories of cited documents:
"A" document defining the general state of the art which is not considered to be of particular relevance
"E" earlier application or patent but published on or after the international filing date
"L" document which may throw doubts on priority claim(s) or which is cited to establish the publication date of another citation or other special reason (as specified)
"O" document referring to an oral disclosure, use, exhibition or other means
"P" document published prior to the international filing date but later than the priority date claimed
"T" later document published after the international filing date or priority date and not in conflict with the applicationbut cited to understand the principle or theory underlying the invention
"X" document of particular relevance; the claimed invention cannot be considered novel or cannot be considered to involve an inventive step when the document is taken alone
"Y" document of particular relevance; the claimed invention cannot be considered to involve an inventive step when the document is combined with one or more other such documents,such combination being obvious to a person skilled in the art
"&" document member of the same patent family

| Date of the actual completion of the international search | Date of mailing of the international search report |
|---|---|
| 25 February 2015 (25.02.2015) | **26 February 2015 (26.02.2015)** |


Name and mailing address of the ISA/KR
**International Application Division**
**Korean Intellectual Property Office**
189 **Cheongsa-ro, Seo-gu, Daejeon Metropolitan City, 302-701, Republic of Korea**
Facsimile No. ++82 42 472 3473

Authorized officer
KIM, Jin Ho
Telephone No. +82-42-481-8699


Form PCT/ISA/210 (second sheet) (January 2015)

**INTERNATIONAL SEARCH REPORT**

Information on patent family members

International application No.

**PCT/US2014/066437**

| Patent document cited in search report | Publication date | Patent family member(s) | Publication date |
|---|---|---|---|
| US 6498942 Bl | 24/12/2002 | AU 6894500 A | 05/03/2001 |
| | | ¥0 01-10295 Al | 15/02/2001 |
| EP 0919180 Al | 02/06/1999 | DE 69837425 T2 | 13/12/2007 |
| | | EP 0919180 Bl | 28/03/2007 |
| | | EP 1795120 Al | 13/06/2007 |
| | | JP 03210632 B2 | 17/09/2001 |
| | | JP 11-235331 A | 31/08/1999 |
| | | KR 10-1999-0045525 A | 25/06/1999 |
| | | TW 408219 A | 11/10/2000 |
| | | us 5941821 A | 24/08/1999 |
| | | us 6049728 A | 11/04/2000 |
| US 5977538 A | 02/11/1999 | EP 1077643 Al | 28/02/2001 |
| | | EP 1077643 Bl | 24/08/2005 |
| | | EP 1535575 Al | 01/06/2005 |
| | | EP 1535575 Bl | 08/04/2009 |
| | | JP 2002-514456 A | 21/05/2002 |
| | | Wo 99-58060 Al | 18/11/1999 |
| US 5840023 A | 24/11/1998 | AU 1997-18570 B2 | 03/05/2001 |
| | | CA 2244732 Al | 07/08/1997 |
| | | CA 2244732 C | 20/04/2010 |
| | | EP 0920277 Al | 06/04/2005 |
| | | EP 0920277 Bl | 14/09/2005 |
| | | JP 11514549 A | 14/12/1999 |
| | | US 6309352 Bl | 30/10/2001 |
| | | us 6405069 Bl | 11/06/2002 |
| | | Wo 00-24315 Al | 04/05/2000 |
| | | wo 97-27801 Al | 07/08/1997 |
| US 5615675 A | 01/04/1997 | AU 1997-25865 B2 | 09/12/1999 |
| | | EP 0904013 Al | 31/03/1999 |
| | | JP 2000-517414 A | 26/12/2000 |
| | | WO 97-39684 Al | 30/10/1997 |